Draft

Measurement of the Ratio G_E^n/G_M^n by the Double-polarized $^2H(\overrightarrow{e}, e'\overrightarrow{n})$ Reaction

An experimental proposal to Jefferson Lab. PAC 45.

May 18, 2017

J.R.M. Annand[1], D.J. Hamilton, K. Hamilton, D.G. Ireland, K. Livingston, I.J.D. MacGregor, R. Montgomery, B. Seitz, D. Sokhan
University of Glasgow, Glasgow G12 8QQ, UK.

B. Wojtsekhowski, A. Camsonne, J.P. Chen, J. Gomez, O. Hansen, D. Higinbotham, M. Jones, C. Keppel, R. Michaels, B Sawatzky
Thomas Jefferson National Accelerator Facility, Newport News, VA 23606, USA.

N. Piskunov, S. Basylev, O. Gavrishchuk, D. Kirillov, G. Meshcheryakov, J. Mushinsky, A. Nagaytsev, I. Savin, I. Slepnev, V. Slepnev, I. Sitnik
Joint Institute for Nuclear Research, Dubna, Russian Federation.

V. Bellini, M. Bondi, P. Castorina, M. De Napoli, A.S. Italiano, V. Kuznetsov, E. Leonora, F. Mammoliti, N. Randazzo, L. Re, G. Russo, M. Russo, A. Shahinyan, C.M. Sutera, F. Tortorici
INFN Catania, Italy.
to be confirmed

M. Kohl, T. Cao, B. Dongwi, A. Liyanage, J. Nazeer, L. Harris
Hampton University, Hampton, VA, USA

E. Brash and P. Monaghan
Christopher Newport University, Newport News, VA, USA

G. Cates, K. Gnanvo, N. Liyanage, V. Nelyubin, H. Nguyen
University of Virginia, Charlottesville, VA 22901, USA

E. Cisbani
INFN Rome, Italy
to be confirmed

[1]Corresponding author: john.annand@glasgow.ac.uk

G. B. Franklin, B. Quinn
Carnegie Mellon University, Pittsburgh, PA 15213, USA

T. Averett, C.A. Gayoso, C. Perdrisat
College of William and Mary, Williamsburg, VA, USA

A. Asaturyan, A. Mkrtchyan, H. Mkrtchyan, V. Tadevosyan, A. Shahinyan, H. Voskanyan, S. Zhamkochyan
A.I. Alikhanyan National Science Laboratory, Yerevan 0036, Armenia

A. J. R. Puckett, E. Fuchey, F. Obrecht
University of Connecticut, Storrs, CT 06269, USA

S. Riordan
Argonne National Laboratory, Argonne, IL 60439, USA

A. Ahmidouch and S. Danagoulian
North Carolina A&T State University, Greensboro, NC 27411, USA

G. Niculescu, I. Niculescu
James Madison University, Harrisonburg, VA 22807, USA

V. Punjabi
Norfolk State University, Norfolk, VA, USA

William Tireman
Northern Michigan University, Marquette, Michigan 49855, USA

Other INFN to be confirmed

and
The Hall-A Collaboration of
Thomas Jefferson National Accelerator Facility.

Abstract

We propose a measurement of double polarized $^2\mathrm{H}(\overrightarrow{e}, e'\overrightarrow{n})$ at a four-momentum transfer $\mathrm{Q}^2 = 4.5$ (GeV/c)^2. The ratio of electric to magnetic elastic form factors $\mathrm{G_E^n/G_M^n}$ will be extracted from the ratio of transverse and longitudinal components of the spin polarization P_x/P_z, which is transferred to the recoiling neutron from an incident, longitudinally polarized electron. The experiment will be performed in Hall-A of Jefferson Laboratory, utilizing common components of the Super BigBite apparatus. It will include apparatus to implement neutron polarimetry, using both $np \rightarrow pn$ (charge-exchange) and $np \rightarrow np$ scattering to analyze the neutron polarization . The electron arm will be the BigBite spectrometer. The hadron arm will be the neutron polarimeter consisting of a Cu block (the analyzer), GEM charged particle trackers, the CDet coordinate detector, the hadron calorimeter HCAL and a set of scintillation counters. The bulk of this apparatus is currently under construction for other approved SBS experiments. The polarimeter will be sensitive both to high-momentum forward-angle protons, to enable it to measure charge-exchange $np \rightarrow pn$ scattering, and to large-angle, low-momentum protons, to enable it to measure $np \rightarrow np$ scattering. A recent measurement at JINR Dubna has shown that $np \rightarrow pn$ on a relatively heavy nucleus has a sizable analyzing power and this measurement will yield valuable information on the figure of merit of the two reaction channels. The present experiment, which we propose to run concurrently with E12-09-019, will yield $\mathrm{G_E^n/G_M^n}$ at the highest Q^2 kinematic point yet recorded. The technical information on the polarimetry will be used to optimize future measurements of $\mathrm{G_E^n/G_M^n}$at in Hall A and/or Hall C to reach Q^2 values as high as 9.3 (GeV/c)^2 using recoil polarimetry techniques.

Contents

1 Introduction **7**
- 1.1 Physics Motivation 7
- 1.2 The scaling behavior of EMFF and non-perturbative QCD . 8
  - 1.2.1 Dyson Swinger Equation Framework 9
  - 1.2.2 Nambu-Jona-Lasinio Model 11
  - 1.2.3 Light Front Holographic QCD 11
  - 1.2.4 The link with Generalized Parton Distributions . . . 11
- 1.3 Previous EMFF Measurements 12
  - 1.3.1 Unpolarized 12
  - 1.3.2 Polarized Target 12
  - 1.3.3 Recoil Polarimetry 13
- 1.4 Related EMFF Measurements at JLab. 13
  - 1.4.1 E12-11-009: *The Neutron Electric Form Factor at Q^2 up to $7 (GeV/c)^2$ from the Reaction ${}^2H(\overrightarrow{e}, e^{'}\overrightarrow{n})$ via Recoil Polarimetry* 13
  - 1.4.2 E12-09-016: *Measurement of the Neutron Electromagnetic Form Factor Ratio* $\mathrm{G_E^n/G_M^n}$ *at high* $\mathrm{Q^2}$ . . 14
  - 1.4.3 E12-09-019: *Precision Measurement of the Neutron Magnetic Form Factor up to $Q^2 = 13.5\ (GeV/c)^2$* . . 14
  - 1.4.4 E12-07-109: *Large Acceptance Proton Form Factor Ratio Measurements at High Q^2 using the Recoil Polarization Method [3].* 15
  - 1.4.5 E12-07-108: *Precision measurement of the Proton Elastic Cross Section at High Q^2* 15
  - 1.4.6 E12-07-104*: Measurement of the Neutron Magnetic Form Factor at High Q2 Using the Ratio Method on Deuterium* 15

2 Double-Polarized Measurements of G_E/G_M **15**
- 2.1 Polarized Beam and Recoil Polarimetry 16
- 2.2 Nucleon Polarimetry 16
  - 2.2.1 Neutron analyzing power at several GeV/c 18
  - 2.2.2 Experimental data for polarized nucleon-nucleon scattering 18
  - 2.2.3 The Figure of Merit for neutron polarimetry 19

3 Experimental Method **21**
- 3.1 The e' Spectrometer BigBite 23
  - 3.1.1 Dipole Magnet 23
  - 3.1.2 Front and Rear GEM Trackers 24
  - 3.1.3 GRINCH Gas Cherenkov 24
  - 3.1.4 Timing Hodoscope 25
  - 3.1.5 Pb-Glass Calorimeter 25
- 3.2 The Neutron Polarimeter 25
  - 3.2.1 The Cu Analyzer 26
  - 3.2.2 The GEM Charged Particle Tracker 26
  - 3.2.3 The HCAL Hadron Calorimeter 27
  - 3.2.4 Rear Detector for Charged-Particle Identification . . 28
  - 3.2.5 Large-Angle Proton Detection 28
  - 3.2.6 The 48D48 Dipole 29

4 Monte Carlo Simulations of the Polarimeter **30**
4.1 Neutron Spin Precession 30
4.2 Separation of neutrons from protons 31
4.3 Polarimeter Angle Reconstruction 32
4.4 Determination of G_E^n/G_M^n from Simulated Azimuthal Asymmetries 34
4.5 Kinematics 36
4.6 Background Rates and the Trigger Rate 37
4.7 Inelastic Background Rejection 40
4.8 Systematic Uncertainties 41

5 Estimates of Experimental Precision **42**

6 Beam Time Request **43**
6.0.1 $Q^2 = 4.5$ (GeV/c)^2 44
6.0.2 $Q^2 = 6.0,\ 9.3$ (GeV/c)^2 44

7 Summary and Comparison with other G_E^n/G_M^n measurements at Jefferson Lab. **45**

Foreword

This proposal builds on the work of LOI12-15-003 and an earlier deferred proposal PR12-12-012. The response of PAC 43 to LOI12-15-003 appears in the final PAC report as follows:

Issues: The TAC raised a number of issues including high rate for the DAQ and backgrounds in the neutron arm. The proposed method in general is the same as what is proposed in the already approved E12-11-009, and the proposed improvement in the FOM of the recoil neutron polarimeter if demonstrated will benefit E12-11-009. There is also an approved Experiment E12-09-016 using a polarized ^{3}He target which allows for an extraction of the neutron electric form factor in excess of Q^2=10 (GeV/c)2 . While the PAC believes in the importance of extending the G_E^n determination from the deuteron to a Q^2 value comparable to that of E12-09-016, the PAC does not believe there should be parallel efforts in pursuing the same experimental technique.

Recommendation: The proponents are encouraged to work with the lab management and the E12-11-009 collaboration to improve the FOM of the recoil neutron polarimeter in order to optimize the measurements using the already approved beam time of E12-11-009.

The SBS and C-GEN (E12-11-009) proponents of $\mathrm{G_E^n/G_M^n}$ by recoil-neutron polarimetry have been discussing neutron polarimetry techniques since the PAC's response to LOI12-15-003 was received. This experiment is aimed at addressing some of the questions (analyzing power, rates, etc....) associated with the $np \to pn$ charge-exchange approach within the SBS apparatus. Experience and data from this staged approach will be used to develop the optimal combination of techniques to measure $\mathrm{G_E^n}$ at the largest Q^2 in either Hall A or Hall C.

In addition, this measurement will, in a relatively short beam time, provide $\mathrm{G_E^n/G_M^n}$ at the highest value of Q^2 yet attained worldwide.. We propose an initial run at a single $Q^2 = 4.5$ (GeV/c)^2 point. This would run concurrently with the $\mathrm{G_M^n/G_M^p}$ experiment, and the kinematic point would be one in the E12-09-019 sequence. The experiment would be adapted to $\mathrm{G_E^n/G_M^n}$ by insertion of polarimeter components on the hadron arm.

While the present proposal requests beam time for one data point only, a study of two additional points at $Q^2 = 6.0, 9.3$ (GeV/c)^2 is included to demonstrate the potential to reach high values of Q^2. This study is based on new measurements of polarized, charge-exchange neutron scattering from nuclei at JINR Dubna. Preliminary results from this experiment confirm that, similar to the free $np \to pn$ case, charge-exchange scattering from nuclei has a high analyzing power at neutron momenta of several GeV/c. This offers a path to high-precision measurements at high Q^2. There is no comparable data on polarized "standard" $np \to np$ scattering and it will be immensely valuable to have this information to determine the optimum setup for future, high-Q^2 operation.

1 Introduction

The understanding of nucleon structure and the nature of quark confinement is one of the central goals facing nuclear physics today. At the $\sim fm$ scales typical of hadrons, quantum chromodynamics (QCD), the field theory describing the quark-gluon interaction, is too strong to be solved by perturbative methods (pQCD) and the understanding of non-perturbative QCD remains a pivotal problem of theoretical physics.

One of the critical factors driving progress in understanding nucleon structure is the availability of high precision electron scattering results over a broad range of Q^2. The higher Q^2 domain is relatively unexplored, especially for the neutron, and thus has immense potential to discriminate between different nucleon structure models. Elastic form factors remain a major source of information about quark distributions at small transverse distance scales and the Q^2 dependence of $\mathrm{G_E^p/G_M^p}$ has generated more theoretical papers than any other result to come out of Jefferson Laboratory (JLab). There is considerable anticipation regarding new results that push both $\mathrm{G_E^p/G_M^p}$ and $\mathrm{G_E^n/G_M^n}$ to higher values of Q^2.

The Super-Bigbite-Spectrometer (SBS) experimental program has three approved measurements of nucleon elastic form factors [1, 2, 3]. In addition E12-07-108 [4] has measured G_M^p up to high Q^2, using the Hall-A HRS spectrometers to achieve a 2-4% measurement of the $e-p$ elastic scattering cross section. In Hall C, a measurement [5] of $\mathrm{G_E^n/G_M^n}$ using the SHMS and a custom neutron polarimeter has been approved. Thus extraction of absolute values of G_M^n, G_E^p and G_E^n from ratio measurements will be possible. A major strength of the JLab program is the ability to measure all four of the Electromagnetic Form Factors (EMFF), with sufficient accuracy and reach in Q^2 to address some of the most fundamental and topical questions in hadronic physics.

We propose a high-precision measurement of $\mathrm{G_E^n/G_M^n}$ at $\mathrm{Q}^2 = 4.5$ (GeV/c)^2, by quasi-elastic $^2\mathrm{H}(\overrightarrow{e}, \mathrm{e}'\overrightarrow{n})$, with the intention of evaluating the best combination of reaction channels and detector systems for measurements at higher Q^2. If a recoil polarimetry experiment can eventually reach $Q^2 = 9.3$ (GeV/c)^2 this will almost triple the Q^2 range currently covered by published data [6] and overlap well with the new experiment E12-09-016 [1]. Ref. [6, 1] both employ $\overrightarrow{^3He}(\overrightarrow{e}, \mathrm{n})$, while existing $^2\mathrm{H}(\overrightarrow{e}, \mathrm{e}'\overrightarrow{n})$ data [7] extend up to $\mathrm{Q}^2 = 1.5$ (GeV/c)^2 only. Neutron measurements are technically very challenging and must employ quasi-free scattering from light nuclei, which introduces some uncertainty in extrapolation to the free-neutron case. However identification of the quasi elastic channel is more straightforward for ^{2}H compared to ^{3}He. By employing different experimental techniques, with different systematic effects, and different light-nucleus ("neutron") targets, with different binding and final state interaction effects, one obtains an extremely valuable cross check on the accuracy of the measurements.

1.1 Physics Motivation

In the one-photon exchange approximation the most general form of a relativistically covariant hadronic current for a spin-1/2 nucleon, which satisfies current conservation, is:

$$J^{\mu}_{hadronic} = e\bar{N}(p')\left[\gamma^{\mu}F_1(Q^2) + \frac{i\sigma^{\mu\nu}q_{\nu}}{2M}F_2(Q^2)\right] \tag{1}$$

where $\bar{N}(p')$ is the nucleon Dirac spinor for the final momentum p', and $F_1(Q^2)$ and $F_2(Q^2)$ are the Dirac (helicity conserving) and Pauli (helicity flip) form factors. It is often convenient to express cross sections and other observables in terms of the Sachs electric (G_E) and magnetic (G_M) form factors which are linear combinations of F_1 and F_2.

$$G_E = F_1 - \tau F_2 \qquad G_M = F_1 + F_2 \tag{2}$$

where $\tau = Q^2/4M_N^2$. G_E and G_M represent, in the Breit frame, the Fourier transforms of the distributions of charge and magnetic moment respectively of the nucleon constituents.

The EMFF (F_1, F_2 or alternatively G_E, G_M) are among the simplest of hadron-structure observables, but none the less they continue to play a vital role in constraining non-perturbative QDC treatments of nucleon structure. Lattice QDC techniques continue to make big strides towards an accurate representation of the EMFF. However calculations of this type are still limited to relatively low values of Q^2 for the nucleon, although for the pion they now overlap well with the kinematic domain accessible at JLab. The EMFF also provide an indispensable constraint to Generalized Parton Distribution (GPD) analyses to extract the "3D" structure of the nucleon as outlined in Sec.1.2.4.

1.2 The scaling behavior of EMFF and non-perturbative QCD

On the basis of quark counting rules F_1 is expected to scale as $1/Q^4$, while F_2 is supposed to scale as $1/Q^6$ [8] at sufficiently high values of Q^2. After publication of Ref.[9], it became clear that F_2^p/F_1^p did not scale as $1/Q^2$, as evident in Fig.1 (Left). The difference in apparent scaling behavior of proton data derived from double-polarized measurements [9, 10, 11, 12, 13], as opposed to Rosenbluth separation of differential cross sections [14, 15, 16], has been attributed to two-photon exchange effects. If these constitute a significant effect, Rosenbluth separation will be highly sensitive, while double-polarized measurements should be relatively insensitive.

The behaviour of the neutron G_E^n/G_M^n ratio (Fig. 2) is quite different from the proton and unknown for $Q^2 > 3.4$ (GeV/c)^2. Measurements of all four Sachs form factors, provide the means to make a flavor separation to obtain the Dirac and Pauli form factors of the u and d quarks: $F^u_{1,2}$, $F^d_{1,2}$ respectively. Assuming negligible nucleon strange content they are linear combinations of the proton and neutron form factors:

$$F^u_{1,2}(Q^2) = F^n_{1,2} + 2F^p_{1,2} \qquad F^d_{1,2}(Q^2) = 2F^n_{1,2} + F^p_{1,2} \tag{3}$$

The kinematic range over which such a separation is possible is limited by the range of G_E^n, which emphasizes the importance of measuring neutron as well as proton distributions with high precision. The first flavor separation [17] to

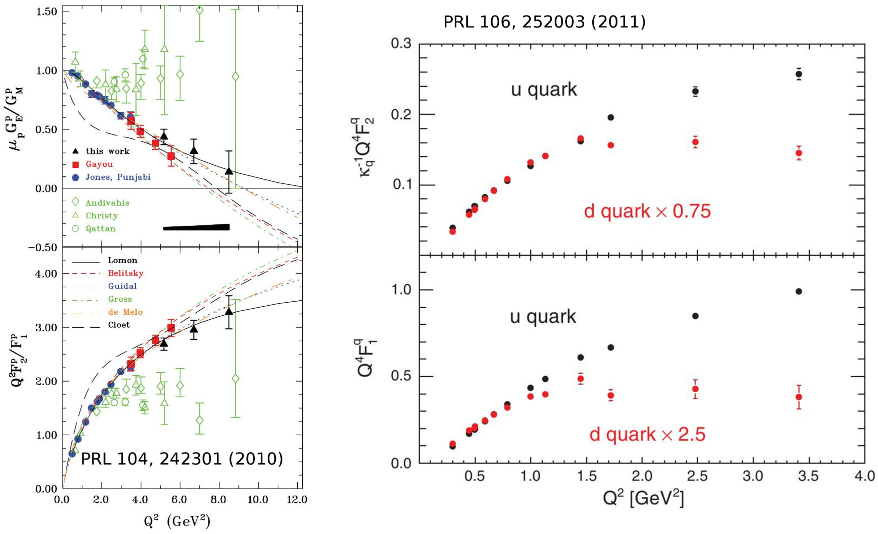

Figure 1: *Left* Q^2 scaling of the proton form factors from Ref[12] compared to theoretical predictions. The blue, red, black data points [9, 10, 12] are JLab double polarized data. The open green data points from SLAC [14] and JLab [15, 16] were obtained by unpolarized Rosenbluth separation. *Right* Q^2 scaling of the separated u, d form factors from Ref. [17].

incorporate Hall-A $\mathrm{G_E^n/G_M^n}$ data [6] up to 3.4 $(\mathrm{GeV/c})^2$ shows an intriguing difference in scaling behavior between the u and d quarks (Fig. 1 Right). Above ~ 1 $(\mathrm{GeV}/c)^2$, $F^d_{1,2}$ appears to scale roughly as $1/Q^4$, whereas $F^u_{1,2}$ appears to scale roughly as $1/Q^2$.

Ultimately lattice QCD is expected to provide the best theoretical description of the Q^2 evolution of the EMFF, and indeed new calculations on the pion [18] reach up to $Q^2 = 6$ $(GeV/c)^2$, coinciding with JLab experiment E12-06-101. However accurate baryon calculations are not possible at medium to high Q^2 as the numerical overheads become too great. Alternatively QCD-compatible calculations of baryon structure may use effective degrees of freedom such as constituent quarks.

1.2.1 Dyson Swinger Equation Framework

One theoretical technique has come to prominence in the past decade. It is based on the infinite series of Dyson-Schwinger Equations (DSE) that interrelate the Green's functions of QCD [19]. Recent calculations explicitly describe the dynamical generation of the mass of constituent quarks, and show excellent agreement with available lattice QCD results. Using the dressed quarks as the elementary degrees of freedom, the nucleon form factors may be calculated using a Poincaré covariant Faddeev equation (DSE/F) [20]. While still an approximation, the DSE/F approach is based on first principles. It is limited, however, in that precisely three constituent quarks are considered, so that for instance pion-cloud effects are not investigated. However, it is reasonable to assume the dominance of the 3-quark component of the wave function at relatively high values of Q^2.

Building on the work of Ref.[20] a unified study of nucleon and Δ elastic and transition form factors has recently been made [21], which provides (Fig. 2) a consistent description of both $\mu_p \mathrm{G_E^p}/\mathrm{G_M^p}$ and $\mu_n \mathrm{G_E^n}/\mathrm{G_M^n}$ and predicts for both a zero-crossing point. The location of the zero crossing point (if it exists) of the ratios has implications for the location and width of the transition region between constituent- and parton-like behavior of the dressed quarks. A more rapid transition from non-perturbative to perturbative behavior pushes the proton zero point to higher Q^2,while conversely the neutron zero point is pushed to lower Q^2. Thus the ability of the JLab EMFF measurements to push into the $Q^2 \sim 10\,(GeV/c)^2$ domain will have a major impact in testing theoretical predictions of this type. In the case of the neutron the kinematic region of interest is completely unexplored.

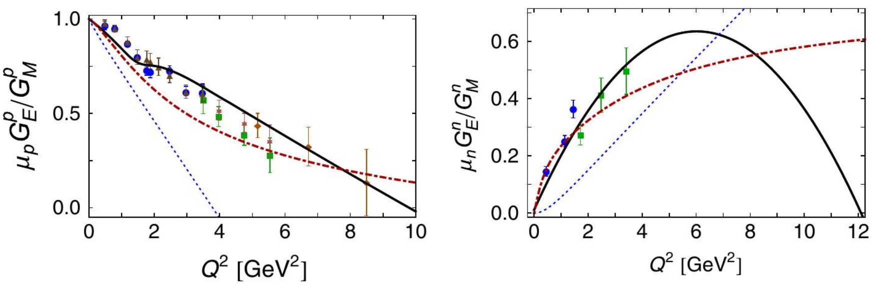

Figure 2: Left: "QCD-kindred" calculation [21] (black line) of $\mu_p \mathrm{G_E^p}/\mathrm{G_M^p}$ compared to JLab data [9, 10, 11, 12, 13]. Right: equivalent calculation of $\mu_n \mathrm{G_E^n}/\mathrm{G_M^n}$ (black line) compared to JLab. data [6, 7]. Red dot-dash lines are from Ref. [57], and blue dotted lines from Ref. [22].

Within the framework of Ref.[21] di-quark correlations are behind the zero-crossing behavior of $\mathrm{G_E}/\mathrm{G_M}$.

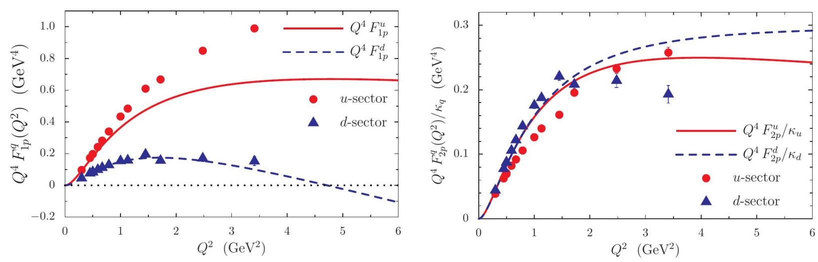

Figure 3: Left: Scaling behavior of F_1 and F_2 for u and d quarks. Data from Ref. [17], curves from the NJL calculation of Ref. [23]

1.2.2 Nambu-Jona-Lasinio Model

Flavor-separated scaling behavior is addressed in Ref. [21] and also in a calculation made within the framework of a covariant, confining Nambu-Jona-Lasinio (NJL) model [23]. For F_1 the dominance of the u-quark sector is interpreted as a consequence of scalar di-quark correlations, which play a smaller role in the d-quark sector. The u-d difference for F_2 is less dramatic, due to axial-vector diquark and pion-cloud contributions to the d sector, counteracting the effect of the scalar di-quark correlation. The comparison with data is limited to $Q^2 \leq 3.4\ (GeV/c)^2$, above which there is no data on G_E^n. Precise new neutron data at $Q^2 > 3.4\ (GeV/c)^2$ and confirmation of the behavior at $1.5 < Q^2 < 3.5\ (GeV/c)^2$ are required to test further these new theoretical developments.

1.2.3 Light Front Holographic QCD

Recently an analysis of the nucleon EMFF has been made within the framework of light-front holographic QCD [24]. The helicity-conserving and helicity-flip current matrix elements required to compute $F_1(Q^2)$ and $F_2(Q^2)$, have an exact representation in terms of the overlap of the nonperturbative hadronic light-front wave functions, the eigen- solutions of the QCD light-front Hamiltonian. As well as elastic form factors, this framework is also capable of predicting hadronic transition form factors, structure functions and the mass spectra of mesons and baryons.

The calculations depicted in Fig. 4 [24] use three adjustable parameters to fit the available proton and neutron form factor data. Two of these give the probabilities of higher Fock states (pion cloud contributions) for $F_2(Q^2)$, which, from comparison with data, are 30% (proton) and 40% (neutron). Departure of the third (parameter r Fig. 4) from unity is interpreted as indicative of SU(6) spin-flavor symmetry breaking effects . The computed curves have an estimated accuracy of $\sim 10\%$, give a good account of the available $\mathrm{G_E}/\mathrm{G_M}$ data for protons and neutrons (with $r = 2.08$) and also describe a u/d flavor separation of F_1 and F_2 as performed in Ref. [25].

Note that, unlike the DSE framework, LFHQCD predicts that $\mu_n \mathrm{G_E^n}/\mathrm{G_M^n}$ rises towards an asymptotic value of ~ 0.85, rather than bending over and decreasing towards zero. Such large differences in theoretical predictions emphasize the importance of collecting neutron data in the $Q^2 \sim 4 - 10\ (\mathrm{GeV/c})^2$ region.

1.2.4 The link with Generalized Parton Distributions

Generalized Parton Distributions (GPD) describe correlations between spatial and momentum degrees of freedom and permit the construction of various types of "3-D images" of the nucleon. The nucleon elastic form factors are critical to the experimental determination of GPDs [26]. In Deeply Virtual Compton Scattering (DVCS), which is generally held to be the optimum channel to access GPD information, the interference between Bethe Heitler and DVCS Handbag mechanisms is measured and the separation of these amplitudes requires EMFF information. The first moments of GPDs are related to the elastic form factors through model independent sum rules:

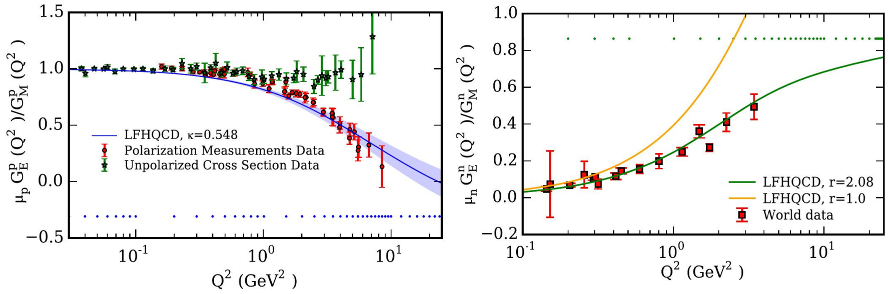

Figure 4: Predictions of Light Front Holographic QCD [24] for the ratios G_E^p/G_M^p (left) and G_E^n/G_M^n (right) .

$$\int_{-1}^{+1} dx H^q(x,\xi,Q^2) = F_1^q(Q^2) \qquad \int_{-1}^{+1} dx E^q(x,\xi,Q^2) = F_2^q(Q^2) \tag{4}$$

These relations are currently some of the most important constraints on the forms of the GPD's and, since it is extremely unlikely that the GPDs will be mapped out exhaustively in the near future, constraints such as those in Eq.4 will be critical to extraction of GPD's. Already the constraints from Eq.4 have played an important role in the first estimates of nucleon quark angular momentum using the Ji Sum Rule and constraining GPDs is in itself an excellent reason to experimentally determine the nucleon elastic form factors.

1.3 Previous EMFF Measurements

1.3.1 Unpolarized

There have been many extractions of the Sachs form factors from Rosenbluth separation of unpolarized differential cross sections. Three of the more recent are given in Ref. [14, 15, 16]. A measurement of proton form factors in Hall-C [15] essentially follows the scaling trend of a previous measurement from SLAC [14]. In Hall-A a proton measurement [16] at Q^2 values of 2.64, 3.20 and 4.10 $(\mathrm{GeV/c})^2$ has also been made, but in this case the differential cross sections were determined by detecting the recoiling proton, in contrast to older measurements where the scattered electron was detected.

Essentially the Rosenbluth extractions all follow $\mu \mathrm{G_E} \sim \mathrm{G_M}$ scaling. They are in definite disagreement with recent polarization transfer measurements of comparable precision (Fig. 1), which has been attributed to the relative sensitivity of Rosenbluth separation to two-photon-exchange effects.

1.3.2 Polarized Target

Vector Polarized ^{2}**H** has the neutron and proton spins aligned in parallel. At NIKHEF a polarized deuterium gas target was used to determine G_E^n at $\mathrm{Q}^2 = 0.21$ [27] via measurement of the spin-correlation parameters. At JLab the range of Q^2 for G_E^n was extended to 0.5, 1.0 $(\mathrm{GeV/c}^{2)}$ [28, 29], using a polarized deuterated ammonia (ND_3) target. For neutron measurements, polarized ^{3}He has the advantage that $\sim 90\%$ of the nuclear polarization is carried by the neutron. At Mainz, a series of polarized ^{3}He target measurements have taken place over a range of $\mathrm{Q}^2 = 0.31 - 1.5$ (GeV/c)^2 [30, 31, 32, 33]. In the GEn(1) experiment at JLab [6] the higher beam energy, high performance ^{3}He target and large acceptance detectors has enabled the Q^2 range to be extended up to 3.4 (GeV/c)^2.

1.3.3 Recoil Polarimetry

There have been several experiments to measure $\mathrm{G_E^n/G_M^n}$ from the polarization of the recoiling nucleon (Sec. 2.1) after scattering of the polarized electron. Proof-of-principle measurements at MIT-Bates [34] were followed by more precise measurements at Mainz. The latter firstly within collaboration A3 [35, 36] and subsequently within collaboration A1 [37]. While the Mainz program was still in progress, experiments at JLab came online, and Hall-C measurements of $\mathrm{G_E^n/G_M^n}$ have been published at Q^2 of 0.45, 1.13 and 1.45 (GeV/c)^2 [7], the last of which is currently the highest value of Q^2 measured by recoil polarization.

The beam energy at pre-upgrade JLab (6 GeV) was significantly higher than Mainz (1.6 GeV) and this has enabled JLab to take the lead in measurements of $\mathrm{G_E^p/G_M^p}$ [9, 10, 12, 13], which now extend to a Q^2 value of 8.5 (GeV/c)^2. This series of measurements has shown conclusively that $\mu G_E \neq G_M$ and may suggest that the ratio crosses zero at some higher value of Q^2. However the precision of the higher Q^2 data points is not sufficient either to pin down that crossing point or to show unambiguously that it exists. The first of these measurements [9] is the most highly cited paper ever published on a JLab experiment.

1.4 Related EMFF Measurements at JLab.

Measurement of the nucleon EMFF will be a major component of Hall-A/SBS experimental programme. The SBS project has three approved EMFF measurements: $\mathrm{G_E^n/G_M^n}$ [1], $\mathrm{G_M^n/G_M^p}$ [2] and $\mathrm{G_E^p/G_M^p}$ [3]. These three measurements, together with a very precise measurement of $\mathrm{G_M^p}$ [4] in Hall A using the HRS Spectrometers, will collectively determine all four nucleon form factors with unprecedented reach in Q^2 and accuracy. In Hall-C an experiment to measure $\mathrm{G_E^n/G_M^n}$ using the SHMS electron spectrometer and a custom built neutron polarimeter has been approved [5] and in Hall-B there is an approved experiment to measure $\mathrm{G_M^n/G_M^p}$ [38].

1.4.1 E12-11-009: *The Neutron Electric Form Factor at Q^2 up to $7(GeV/c)^2$ from the Reaction $^2H(\overrightarrow{e}, e^{'}\overrightarrow{n})$ via Recoil Polarimetry*

This measurement of $\mathrm{G_E^n/G_M^n}$ [5] from quasi-elastic $^2\mathrm{H}(\overrightarrow{e}, \mathrm{e}'\tilde{\mathrm{n}})$ has been approved for Hall-C using the Super High Momentum Spectrometer (SHMS) and a custom built neutron polarimeter (NPOL). At present, the polarimeter registers $n-p$ interactions in a series of segmented plastic-scintillator analyzers and detects recoiling protons in top and bottom segmented arrays of $\delta E{-}E$ counters. This current geometry is optimized to detect a relatively low momentum, large-angle recoiling proton after n-p scattering. The C-GEN collaboration is investigating a variety of options to increase sensitivity to the charge-exchange channel within NPOL to maximize the FoM for Q^2 values beyond those of the initially approved experiment. Members of the C-GEN collaboration have joined the present proposal because of interest in understanding the analyzing power and systematics for small-angle recoiling protons from the charge-exchange channel, as well as the opportunity to study aspects of the large-angle recoiling protons within the same aparatus.

1.4.2 E12-09-016: *Measurement of the Neutron Electromagnetic Form Factor Ratio* $\mathrm{G_E^n/G_M^n}$ *at high* Q^2

This experiment [1] will measure the double-spin asymmetry in quasi-elastic $\overrightarrow{^3He}(\overrightarrow{e},\mathrm{e'n})\mathrm{pp}$ using a new highly-polarized ^{3}He target, capable of withstanding beam currents up to 60 μA. The scattered electron will be detected in BigBite and the recoiling neutron in a hadron calorimeter (HCAL). Measurements are proposed at $\mathrm{Q}^2 = 1.5$, 3.7, 6.8, 10.2 $(\mathrm{GeV/c})^2$, which can be compared to the current highest GEn(1) point at $\mathrm{Q}^2 = 3.4$ $(\mathrm{GeV/c})^2$. Accurate new $\mathrm{G_E^n/G_M^n}$ data at medium-high Q^2will have enormous physics impact. Clean separation of the QE signal from inelastic background is considerably more challenging for ^3He compared to ^2H and nuclear-medium effects for a neutron bound in ^3He will also be larger. Development of the polarized ^3He target is making good progress, but never the less it will be a major challenge to maintain the predicted 60% polarization with an incident 60 μA electron beam.

Although E12-09-016 can in principle achieve superior precision to a recoil-polarimetry experiment, its systematic uncertainties will be considerably larger and confirmation of its results by recoil polarimetry, a different experimental technique, will be extremely important.

1.4.3 E12-09-019: *Precision Measurement of the Neutron Magnetic Form Factor up to* $Q^2 = 13.5$ $(GeV/c)^2$

In experiment E12-09-019 [2] the combination of high precision measurements of $\mathrm{G_M^p}$ and $\mathrm{G_M^n}$ will permit the reconstruction of the individual u and d quark distributions with an impact-parameter resolution of 0.05 fm. These data are needed both to determine the $u-d$ difference and to study the QCD mechanisms which govern these distributions. $\mathrm{G_M^n/G_M^p}$ will be obtained from the cross-section ratio of $^2\mathrm{H(e,e'n)}$ and $^2\mathrm{H(e,e'p)}$ quasi-free scattering from the deuteron. This ratio method has also been proposed using CLAS12 (Sec. 1.4.6) which can measure on a fine grid of Q^2 points. However, the SBS measurement can be made at much higher luminosity and can achieve superior precision at high Q^2. The HCAL calorimeter for the SBS measurement offers very similar proton and neutron detection efficiencies which are close to 100%. This suppresses a potential major source of systematic uncertainty in the ratio method.

The proposed apparatus for the present experiment is just the E12-09-19 apparatus, with the inclusion of the neutron polarimeter.

1.4.4 E12-07-109: *Large Acceptance Proton Form Factor Ratio Measurements at High Q^2 using the Recoil Polarization Method [3].*

This experiment will measure the ratio $\mathrm{G_E^p/G_M^p}$ at $\mathrm{Q^2} = 5, 8, 12$ $(\mathrm{GeV/c})^2$ with a relative uncertainty of ~ 0.1, which should confirm the zero-crossing point in Q^2, if it exists. The experiment will use the 11 GeV polarized electron beam, a 40 cm long liquid hydrogen target, the BigCal electromagnetic calorimeter to detect the elastically scattered electrons and SBS, equipped as a polarimeter, for the detection of the recoiling proton. A luminosity of $\sim 10^{39}$ will be necessary to reach the desired precision, and the technical solutions to the problems imposed by high rates in the detectors will be of general benefit to the SBS programme.

The present experiment will use the same GEM trackers and hadron calorimeter designed originally for the E12-07-109 polarimeter.

1.4.5 E12-07-108: *Precision measurement of the Proton Elastic Cross Section at High Q^2*

This experiment [4] used the two Hall-A HRS to perform a high precision (2-4%) measurement of $H(e, e'p)$, over a range of Q^2 up to 13.5 $(GeV/c)^2$. This experiment ran in 2016 and the data will yield high precision values of G_M^p. The original goal was to reach Q^2 up to 17.5 $(GeV/c)^2$. However as the highest beam energies were not available during the 2016 run, it was not possible to reach the highest proposed Q^2 values. Never the less a value of 13.5 $(GeV/c)^2$ is still as big as that currently approved in any SBS experiment.

1.4.6 E12-07-104*: Measurement of the Neutron Magnetic Form Factor at High Q2 Using the Ratio Method on Deuterium*

This measurement of the $\mathrm{G_M^n/G_M^p}$ ratio has been proposed using CLAS12 [38]. Compared to E12-09-019 (Sec. 1.4.3) this experiment can measure in one setting a broad kinematic range on a fine grid of $\mathrm{Q^2}$ points. By contrast E12-09-019 will measure at several discrete kinematic settings on a coarser grid, but can achieve higher experimental luminosity.

2 Double-Polarized Measurements of G_E/G_M

The double polarization method for the measurement of G_E was originally proposed [39] to improve the experimental sensitivity to the spin-flip form factor $\mathrm{F_2}$ at large momentum transfer, and subsequent work [40] developed the formalism. A number of form-factor measurements have been performed in recent years: either with polarized nucleon targets, or with a polarimeter to measure the polarization transfer to the recoiling nucleon. The technique of choice depends on the comparison of achievable luminosity, detector efficiency, detector acceptance and the experimental asymmetry, which in turn depends on the target polarization or polarimeter analyzing power.

In the case of the neutron, quasi-elastic scattering from the neutron bound in ^{2}H or ^{3}He offers the nearest approximation to the free scattering case. Bound-nucleon and final-state-interaction effects become less important as momentum transfer increases above $\sim 1(\mathrm{GeV/c})^2$ [41], but none the less it is highly desirable to have data on both targets to check consistency. Neutron measurements are inherently more challenging than their proton equivalents, as demonstrated by their more restricted kinematic range $\mathrm{G_E^n/G_M^n}$: $\mathrm{Q}^2 \leq 3.4$ (GeV/c)^2 as opposed to $\mathrm{G_E^p/G_M^p}$: $\mathrm{Q}^2 \leq 8.5$ (GeV/c)^2. High precision measurements of $\mathrm{G_E^n/G_M^n}$ at $\mathrm{Q}^2 = 4.5$ (GeV/c)^2, followed by measurements as high as 9.3 (GeV/c)^2, will have extremely high selectivity of the quite diverse predictions of different theoretical models. Thus it is extremely important to have reliable, independently verified neutron results.

Whether working with a polarized target or a recoil polarimeter, the ability to separate G_E from G_M and the relative freedom from possible two-photon exchange effects make double-polarization asymmetry measurements the techniques of choice for accessing G_E^n.

2.1 Polarized Beam and Recoil Polarimetry

For a free nucleon the polarization transferred from the electron to the nucleon can be written as:

$$P_x = -hP_e \frac{2\sqrt{\tau(1+\tau)}\tan\frac{\theta_e}{2} G_E G_M}{G_E^2 + \tau G_M^2(1+2(1+\tau)\tan^2\frac{\theta_e}{2}} \tag{5}$$

$$P_y = 0 \tag{6}$$

$$P_z = hP_e \frac{2\tau\sqrt{1+\tau+(1+\tau)^2\tan^2\frac{\theta_e}{2}}\tan\frac{\theta_e}{2} G_M^2}{G_E^2 + \tau G_M^2(1+2(1+\tau)\tan^2\frac{\theta_e}{2})} \tag{7}$$

$$\frac{P_x}{P_z} = \frac{1}{\sqrt{\tau+\tau(1+\tau)\tan^2\frac{\theta_e}{2}}} . \frac{G_E}{G_M} \tag{8}$$

where h and P_e are the helicity and polarization respectively of the electron beam. Eq.8 requires the measurement of the longitudinal component of the neutron polarization P_z and this must be precessed into the transverse plane. The angle of precession through a magnetic field may be expressed as

$$\chi = \frac{2\mu_n}{\hbar c}\frac{1}{\beta_n}\int_L \mathbf{B}.dl \tag{9}$$

where $L(x, y, z)$ is the path through the field, $\mathbf{B} = (B_x, B_y, B_z)$ is the flux density, μ_n is the neutron magnetic moment and β_n is the neutron velocity. With a horizontal field $(B_x, 0, 0)$ the spin will precess in the $y - z$ plane (See Sec.2.2).

2.2 Nucleon Polarimetry

Nucleon polarimetry depends on the spin-orbit interaction of an incident nucleon with a target nucleon or nucleus, which produces an azimuthal modulation of the scattering cross section:

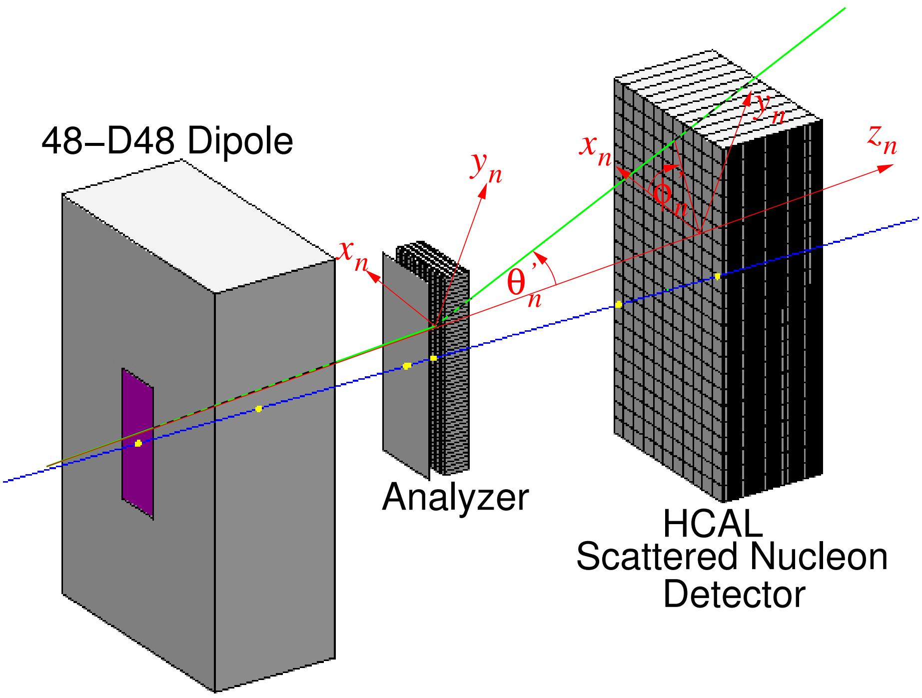

Figure 5: Schematic view of a neutron polarimeter, using SBS detector components

$$\sigma(\theta_n^{'}, \phi_n^{'}) = \sigma(\theta_n^{'}) \left[1 + A_y(\theta_n^{'}) \left\{ P_x^n \sin\phi_n^{'} + P_y^n \cos\phi_n^{'} \right\}\right] \tag{10}$$

where $\sigma(\theta_n^{'})$ is the unpolarized scattering differential cross section, $A_y(\theta_n^{'})$ is the analyzing power of the scattering process and P_x^n, P_y^n are respectively the horizontal and vertical components of the incident nucleon polarization. Scattering angles are shown in Fig.5. The effectiveness of any polarimeter will depend on a combination of its detection efficiency and analyzing power, which can be parametrized as a Figure of Merit (FoM) $\mathcal{F}$ given by:

$$\mathcal{F}^2(p_n) = \int \varepsilon(p_n, \theta_n^{'})\, A_y^2(p_n, \theta_n^{'}) d\theta_n^{'} \tag{11}$$

where $\varepsilon(p_n, \theta_n^{'})$ is the detection efficiency which depends on the cross section for the scattering process and the thickness of the polarimeter material. The angular range is determined by the polarimeter geometry and obviously good acceptance for the region where A_y is large is important. The thickness is usually limited in practice by multiple scattering considerations, as with multiple scattering the initial scattering plane is lost. If $\mathcal{F}$ is known then the precision of the obtained incident polarization may be obtained from:

$$\Delta P = \sqrt{\frac{2}{N_{inc}\mathcal{F}^2}} \tag{12}$$

where N_{inc} is the number of incident particles. Note that the polarimeter proposed here (Sec. 3.2) has a large azimuthal coverage up to polar angles of $\sim 15°$, which will contain most of the useful forward angle scattering. This is also advantageous for untangling the P_x and P_y polarization components.

Note that in measuring the ratio P_x/P_z (Eq.8) the analyzing power cancels, assuming that it is independent of the relative x and y components of polarization. It is however important to have a reasonable estimate of the analyzing power in order to predict the running time required to reach a given precision.

2.2.1 Neutron analyzing power at several GeV/c

Neutron polarimetry is generally based on free elastic $n-p$ scattering or elastic-like $n-p$ scattering from nuclei, where the detected proton is used to reconstruct the scattering kinematics. Elastic-like $n-n$ scattering from nuclei can also be used in principle, but in practice it is difficult or impossible to reconstruct the scattering kinematics if it is associated with a very low energy recoiling charged particle. This is necessary to select the range of polar angles where the analyzing power is relatively large (Eq.11). In comparison to proton scattering, the analyzing power A_y for neutron polarimetry at GeV energies is poorly known. Free $n-p$ scattering is in principle the best analyzer of neutron polarization, but the use of a hydrogen analyzer is challenging technically and up to now scattering from C or CH_2 has generally been used. However A_y for elastic-like scattering from nuclei is lower than the free-scattering case.

In the following the available experimental evidence (Sec. 2.2.2) is presented.

2.2.2 Experimental data for polarized nucleon-nucleon scattering

Information on polarized nucleon scattering for incident momenta $p_N \gtrsim 1.5$ GeV/c is presented in Fig. 7 A. This comes from a number of sources.

1. Measurements of the asymmetries of the $d(\vec{p}, p')n$ and $d(\vec{p}, n)p$ processes have been performed in the 1970s [43, 44] which, in the case of the former, are consistent with elastic $\vec{p} + p \rightarrow p + p$ measurements [45]. These experiments measured both $p-p$ and $p-n$ scattering.

2. Inclusive measurements of $\vec{p}+\mathrm{CH}_2 \rightarrow p+X$ [46], and $\vec{p}+\mathrm{C} \rightarrow p+X$ [47, 48] have been obtained in the calibration of proton polarimeters used at ANL, JINR Dubna and JLab.

3. Measurements of the asymmetries of polarized charge exchange $n + \vec{p} \rightarrow p + X$ scattering [49, 50], have also been made at ANL in the 1970s.

4. A measurement of polarized charge-exchange $\vec{n}+A \rightarrow p+X$ [51] has been made for C, CH, CH2 and Cu targets at incident momenta ~ 4 GeV/c in November 2016 and February 2017 at JINR Dubna (Sec. 7).

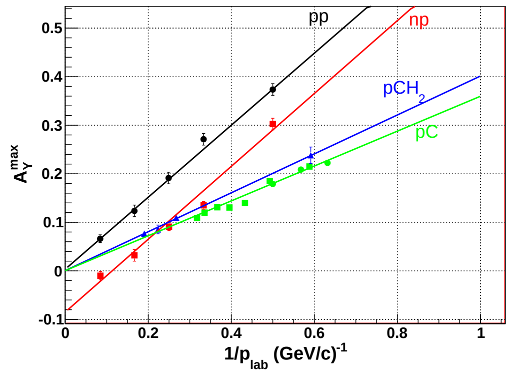

Figure 6: The dependence of the maximum of A_Y on $1/p_{lab}$. Black circles: ANL $d(\vec{p}, p')n$ data [43, 44]; black line: linear fit. Red squares: ANL $d(\vec{p}, n)p$ data [43, 44]; red line: linear fit. Blue triangles [46]: $\vec{p} + \mathrm{CH}_2 \rightarrow charged + X$; blue line: linear fit [46]. Green squares [47] and circles [48]: $\vec{p} + \mathrm{C} \rightarrow charged + X$; green line: linear fit [46].

Fig.6 displays the maximum values of the angle-dependent polarization asymmetries of $p-p$ and $p-n$ scattering, as determined from the data of Ref.[43, 44, 46, 47, 48] and plotted in as a function of $1/p_{lab}$. The main features include the negative offset of the $p-n$ data with respect to $p-p$. The factor 2 reduction in the analyzing power of quasi-free (^{12}C) with respect to free $p-p$ scattering is presumably similar for $n-p$ scattering, but to our knowledge there are no data on polarized $n-p$ scattering from nuclei in the multi-GeV energy domain.

From (Fig. 7 top) it is evident that $p-n$ (equivalent to $n-p$) polarization is dependent on incident nucleon momentum p_{lab}, as well as t, where $-t$ is the squared four-momentum transfer. On the other hand charge-exchange $n-p$ (Fig. 7 Bottom) is t-dependent, with a large polarization at sufficiently large $-t$, but given the spread in the data there is no apparent strong dependence of A_y on p_{lab}. New polarized, charge-exchange data from JINR Dubna [51] (Sec. 7) also show a sizable asymmetry, but an assessment of the reduction factor in analyzing power, compared to the free-scattering case, awaits a more detailed analysis.

2.2.3 The Figure of Merit for neutron polarimetry

Neutron-polarimeter FoM values (Eq. 11) have been calculated over a range of p_{lab} for both charge-exchange $n-p$ and $n-p$ scattering.

Elastic-like $p-p$ scattering from nuclei is observed to have a factor-two reduction in A_Y compared to the free elastic $p-p$. For $n-p$, an application of the same reduction factor is consistent with the polarimeter analyzing power obtained in a previous JLab measurement of G_E^n/G_M^n [7] at 1.45 GeV/c. The value of A_y for free, elastic $n-p$ scattering has been calculated from a fit [52] (Fig. 7) to the $p-n$ data. For charge-exchange $n-p$ scattering from Cu, A_y is taken from a preliminary analysis of new data from Dubna (Sec. 7). This analysis has given the dependence of A_y on $p_t = p_{lab} \sin\theta_{np}$ at an incident momentum

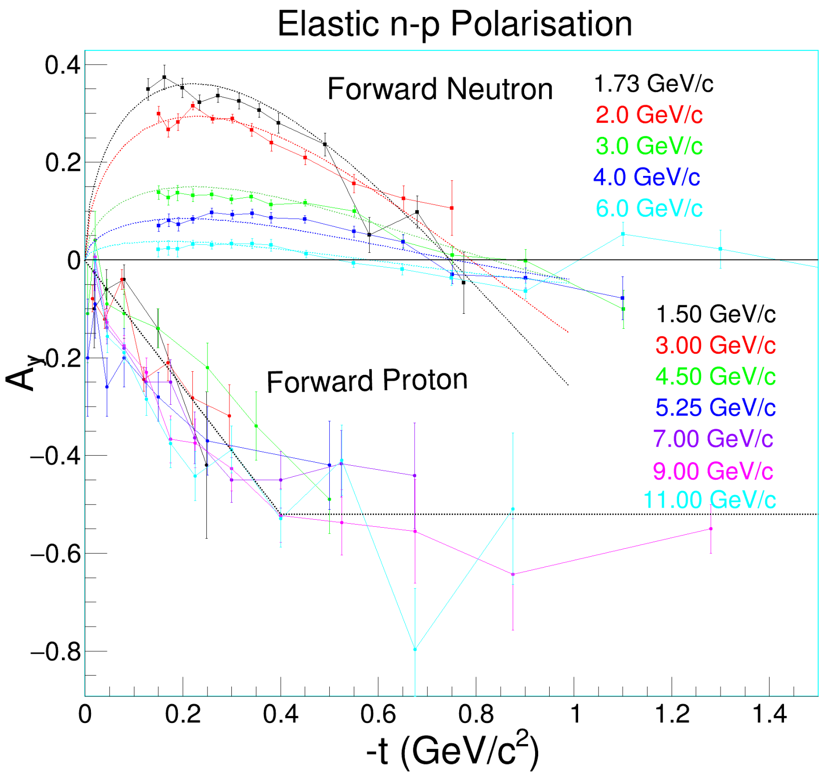

cd

Figure 7: Top: the p_{lab} and t-dependence of the polarization of $p-n$ scattering [43, 44]. The smooth dotted lines show the fit of Ref. [52] to the $p-n$ data. Bottom: the p_{lab} and t dependence of charge-exchange $n-p$ scattering [49, 50]. The color coding relates the data to momentum labels.

of 3.75 GeV/c. A_y is dependent on p_t, but has been assumed independent of p_{lab}, in a manner consistent with the free charge-exchange $n-p$ data (Fig. 7). Polarimeter efficiencies have been calculated using Monte Carlo (MC) simulations of the polarimeter which record the differential detection efficiency as a function of scattering angle. The MC generated data have been filtered according to cuts on energy and angle (Sec. 11,4.3).

Calculations have been made for two versions of the polarimeter compatible with the SBS apparatus.

1. The polarimeter uses the proposed Cu analyzer with forward-angle proton detection by GEM trackers and hadron calorimeter.

2. The polarimeter employs an active position sensitive CH (plastic-scintillator) analyzer with forward angle neutron detection by the hadron calorimeter.

At neutron momenta above ~ 3.5 GeV/c, the FoM from charge-exchange $n-p$ starts to dominate standard $n-p$ and by ~ 6 GeV/c it is projected to be a factor ~ 15 larger. The present experiment will verify if these projections are accurate at $p_n = 3.15$ GeV/c and allow for a real-world evaluation of systematics associated with using the charge-exchange channel to extract G_E^n at Q^2 =4.5 (GeV/c)^2 and beyond.

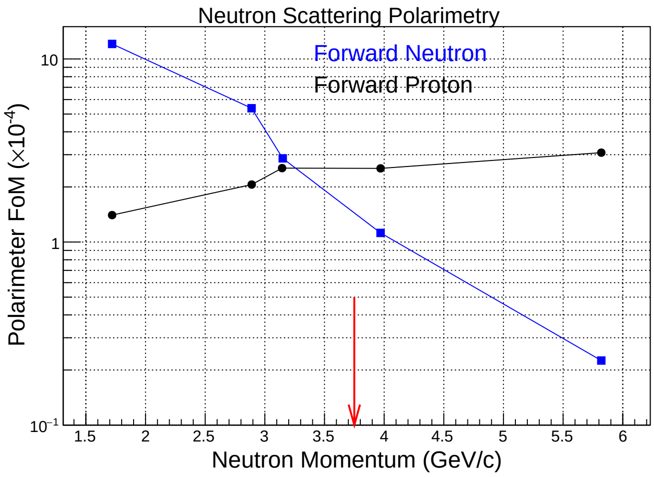

Figure 8: Neutron polarimeter figure of merit as a function of incident neutron momentum for two styles of polarimeter within the SBS apparatus using preliminary data from the recent Dubna measurement. Blue squares: standard $n-p$ scattering from CH scintillator, black circles: charge-exchange $n-p$ scattering from Cu. The red arrow marks the neutron momentum at which a charge-exchange measurement of the analyzing power of Cu was made at Dubna.

3 Experimental Method

The recoil polarization technique requires a large number of counts, because of the relatively low analyzing power of the polarimeter. Going to high momentum transfer, where the elastic scattering rate scales approximately as $\mathrm{E}_{\mathrm{beam}}^2/\mathrm{Q}^{12}$, requires high luminosity, large acceptance and a high rate capability in the detection system. A plan view of the detector apparatus is displayed in Fig.9.

Almost all of the detectors of the present proposal are already under construction for other SBS experiments. Most of the apparatus is identical to that used in the approved $\mathrm{G_M^n/G_M^p}$ experiment E12-09-019, which will undergo a JLab "Readiness Review" in June 2017.

- The same LD_2 target and beam line is used.
- The luminosity at 1.25×10^{38} $cm^2 s^{-1}$ is the same.
- The same BigBite spectrometer on the e' arm is used and the configuration of the detector is identical.
- The same 48D48 dipole on the hadron arm is used.

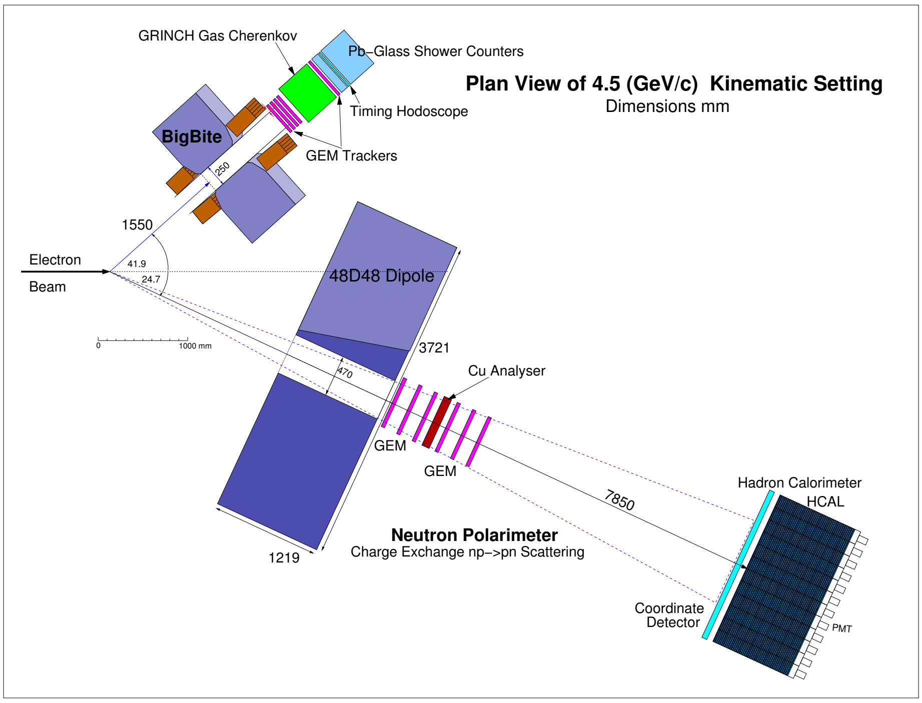

Figure 9: Plan view of experiment $Q^2 = 4.5\ (\mathrm{GeV/c})^2$.

- The same HCAL hadron calorimeter is employed for the detection of energetic protons and neutrons.
- The same CDet coordinate detector is used in front of HCAL for additional particle and position identification.

G_{En}/G_{Mn} experiment E12-09-016 will also use the detectors and dipole itemized above. The additional GEM tracking detectors for the present neutron polarimeter are also used in the proton polarimeter of $\mathrm{G_E^p/G_M^p}$ experiment E12-07-109, but the Cu analyzer block and additional large-angle proton detectors will be new.

We propose to perform the measurement in Hall-A of Jefferson Laboratory, using the CW, polarized electron beam from the CEBAF accelerator. This has a maximum energy of 11 GeV and maximum current of 80 μA. The present experiment will use a beam energy of 4.4 GeV (Table 3) an integral factor of a the standard 2.2 GeV energy gain per pass around the race track. Beam polarizations in excess of 80% have been achieved routinely during 6 GeV operation of CEBAF and 80% is assumed for estimates of precision in measuring form factor ratios.

The electrons will be incident on a 10 cm long liquid deuterium (LD_2) target with 100 μm Al entrance and exit windows, giving ~ 0.054 g/cm^2 of material, compared to ~ 1.69 g/cm^2 for the LD_2. A liquid hydrogen (LH_2) target will also be used for calibrations. A 40 μA electron beam incident on a 10 cm LD_2 target produces an electron-neutron luminosity of $\sim 1.26 \times 10^{38}$ cm^{-2}s^{-1}.

Scattered electrons are detected in the BigBite spectrometer, which will reconstruct the momentum, direction and reaction vertex, as well as correlating the trigger time to an accelerator beam bunch . The neutron arm will be a polarimeter which consists of a Cu analyser, preceded and followed by sets of GEM trackers, and the hadron calorimeter HCAL. The polarimeter will provide position and time-of-flight information for the recoiling nucleon, as well as scattering asymmetries. Neutron spin precession will be performed by the "48D48" dipole which is the basis of the SBS charged-particle spectrometer. The experimental components are described in more detail in the following subsections.

3.1 The e' Spectrometer BigBite

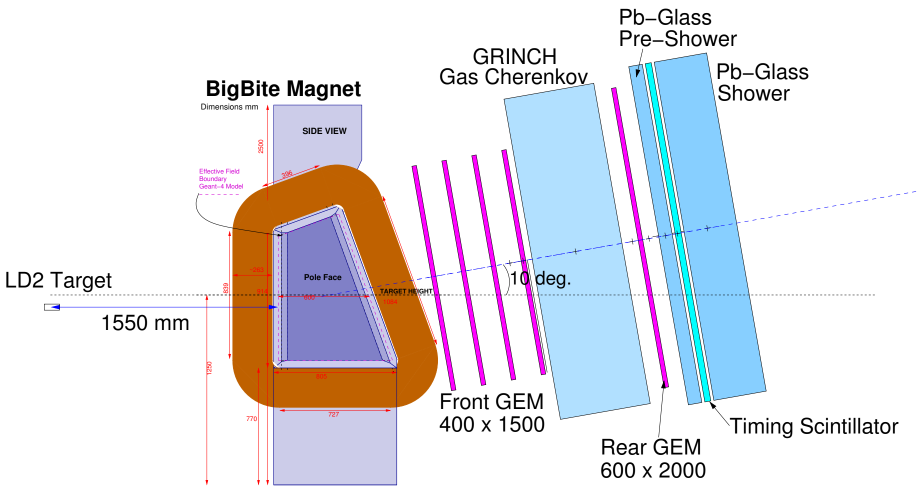

Figure 10: The BigBite electron spectrometer

BigBite is a large-acceptance, non-focusing magnetic spectrometer which, when positioned with the entrance aperture of the dipole 1.55 m from the target center, subtends a solid angle of ~ 58 msr. The configuration of BigBite for the present experiment would be identical to that of experiment E12-09-019 to measure G_M^n/G_M^p and experiment E12-09-016 to measure G_E^n/G_M^n. The components of BigBite are described in the following.

3.1.1 Dipole Magnet

The 20 ton dipole, constructed at the Budker institute, was used originally at NIKHEF and has been used in several experiments performed with the 6 GeV CEBAF accelerator. With the entrance aperture at 155 cm from the target center, the minimum central scattering angle that BigBite can reach (limited by the proximity of the exit beam line) is around 30 deg. The maximum integrated field is 1.2 Tm, so that for GeV electrons the bend angle is relatively small, approximated by:

$$\theta_e \approx \frac{0.3 \int B.dl}{p_e} \tag{13}$$

where the field integral is in Tm and the electron momentum in GeV/c. The angular uncertainty of the deflected electrons from the coordinate resolution of the tracker, taking multiple Coulomb scattering into account, may be estimated for relativistic electrons as

$$\delta\theta = \sqrt{\left(\frac{\sigma_r}{z_{tr}}\right)^2 + \left(\frac{13.6}{p_e}\sqrt{\frac{x}{X_0}}\left[1 + 0.038\ln\left(\frac{x}{X_0}\right)\right]\right)^2} \tag{14}$$

where p_e is the electron momentum in MeV/c and x/X_0 is the thickness of intervening material in radiation lengths. The materials in the front tracking system (Sec.3.1.2) amount to $x/X_0 \sim 0.017$ and the angular uncertainty from the tracking coordinate resolution is ~ 0.5 mr. This translates to an angular resolution of (in both dispersive and non-dispersive directions) of $\delta\theta \sim 1.4$ mr at $p_e = 1.14$ GeV/c and $\delta\theta \sim 0.6$ mr at $p_e = 3.81$ GeV/c.

The momentum resolution $\delta p/p \sim 0.5\%$ will be adequate to identify quasi-elastic scattering in the present experiment (Sec.4.7). The z-vertex resolution at the target is around ~ 2 mm. It is extremely important to have an accurate knowledge of the vertex and direction of the virtual photon, so that the BigBite optics and vertex reconstruction will be calibrated at each kinematic setting, using a sieve slit and multi-carbon-foil target. Momentum will be calibrated using elastic $e-p$ scattering from a LH_2 target.

3.1.2 Front and Rear GEM Trackers

The GEM trackers supersede the MWDC, used in experiments during the 6 GeV CEBAF era, and offer increased counting rate capability, so that higher experimental luminosities may be achieved.

The front GEM trackers are under construction at INFN Rome (Sanita). They are based on triple-foil GEM modules each 40×50 cm in area, grouped in threes to give an area of 40×150 cm per tracking plane. The 2D readout strips are pitched at 0.4 mm which give a coordinate resolution of 0.070 mm. Readout of the strips is performed by the APV25 ASIC which records the strip charge at a sampling rate of 40 MHz (25 ns per sample) and the start time can be reconstructed to ~ 5 ns precision.

The rear GEM tracker is under construction at The University of Virginia (UVa). It is similar to the front GEMs, but each module is 60×50 cm in area and the single plane will be constructed from 4 modules to give an area of 60×200 cm. The pitch of the readout strips is the same as for the front GEMs, so that these planes will also have a coordinate resolution of ~ 0.07 mm. Readout of the strips will also be by the APV25 chip.

Front and rear trackers will be separated by the GRINCH gas Cherenkov counter.

3.1.3 GRINCH Gas Cherenkov

Separation of e^- from π^- particles will be performed by the "GRINCH" gas Cherenkov counter which being constructed at The College of William and Mary (W&M). Light is collected by four cylindrical mirrors and reflected on to a set of 510 9125 PMT's, which have a diameter of 29 mm. Compared to the previous BigBite gas Cherenkov, which used 130 mm PMTs, the new detector will have superior counting rate capability and will be much less susceptible to soft background from the electron beam line. Photons produced by electron tracks through the gas will produce clusters of hits in adjacent PMTs which will be identified by time coincidence. Work is in progress to include GRINCH signals in the BigBite trigger. By suppressing events from non-electron charged particles and energetic photons from π^0 decay the experimental trigger rate will be reduced considerably (Sec. 4.6). The chamber will operate at just above 1 atm pressure and the standard gas will likely be C_4F_{10} ($\eta = 1.0015$), which has a π^- threshold of $\sim$ 2.5 GeV/c at 1 atm , but CO_2 ($\eta = 1.00045$), would also be possible for higher momentum operation, giving a π^- threshold of $\sim$ 4.6 GeV/c

3.1.4 Timing Hodoscope

Timing from BigBite is provided by a plastic scintillator hodoscope. For high luminosity operation a new, finer granularity, hodoscope is being constructed by The University of Glasgow (UGla). This will consist of 90 EJ200 plastic scintillator bars, dimensions 25×25×600 mm, each read out by 2, ET9142 29 mm photomultipliers (PMT). The intrinsic timing resolution of this device, measured with cosmic-ray muons, is 0.15 ns, which will allow correlation with single RF beam bucket from the CEBAF accelerator, which operates at 750 MHz.

3.1.5 Pb-Glass Calorimeter

BigBite is equipped with lead glass Cherenkov pre-shower and shower counters to provide a trigger which is insensitive to low energy background, but has a high efficiency for the electrons of interest. They are the same detectors used with BigBite for 6 GeV experiments. The pre-shower counter are oriented with their long axes perpendicular the electron direction and correlation of their signal amplitude with that from the shower counters provides an additional means to distinguish electrons from π^-.

3.2 The Neutron Polarimeter

The neutron polarimeter (Fig. 9) consists of five main components:

1. The 48D48 dipole magnet
2. A $60 \times 200 \times 4$ cm block of Cu to act as the polarization analyzer.
3. Three 60x200 cm GEM chambers situated in front of the analyzer to detect and momentum analyze protons produced in the deuterium target.
4. Three 60x200 cm GEM chambers situated after the analyzer to detect and track protons produced by n-p charge-exchange, or $p-p$ scattering in the analyzer.
5. The segmented hadron calorimeter HCAL, which is optimized to detect nucleons with momenta of 1.5 - 10 GeV/c with high efficiency.

6. The coordinate detector situated immediately in front of HCAL to aid particle identification and HCAL proton hit-position determination

7. Large angle proton detector

3.2.1 The Cu Analyzer

Material	Z	A	ρ (g/cm^3)	ρ_p (N_A/cm^3)
C	6	12.00	2.26	1.13
Al	13	26.98	2.70	1.30
Fe	26	55.85	7.87	3.22
Cu	29	63.55	8.96	4.09
W	74	183.85	19.30	7.76
Pb	82	207.19	11.35	4.49

Table 1: Comparison of the "proton density" ρ_p of common structural materials, where N_A is the Avogadro constant.

Cu has been chosen as the analyzer material as it has a high number of protons per unit volume, which enables reasonable polarimeter efficiency to be obtained with a 4 cm thick analyzer block. By contrast a C or CH_2 would be much thicker to achieve similar efficiency. A thin analyzer gives more accurate kinematic reconstruction of the neutron interaction position, through tracking of the protons produced after charge-exchange $n-p$ scattering. Of the commonly used structural materials, W has the highest proton density, but Cu has been chosen as there is new empirical evidence of the analyzing power of the charge-exchange $n-p$ scattering process. Although on preliminary evidence the analyzing powers of C and Cu are similar (Sec.7), there is no data to show that this insensitivity to Z extends to heavy nuclei. Large area Cu sheet is also more readily available and cheaper than bulk W material.

3.2.2 The GEM Charged Particle Tracker

The analyzer is preceded and followed by two GEM tracking systems, each consisting of 3 planes of 60 $\times$ 200 cm area. These detectors, which have a coordinate resolution of 0.07 mm, are identical to the GEM plane which forms the rear tracker of BigBite (Sec. 3.1.2). They also form the tracking system for the proton polarimeter of experiment E12-07-109. The front set of GEM chambers identifies protons produced in the deuterium target, while the rear set identifies protons from charge-exchange $n - p$ and $p - p$ scattering in the analyzer. While $n - p$ scattering is of primary interest to this proposal, the ability to record $p-p$ scattering also provides the potential to measure a proton asymmetry.

With a charged track on either side of the analyzer, the accuracy of the reconstruction of the hit position at the analyzer, on the basis of the exit track only (as will be the case for charge-exchange $n - p$), can be checked. The correlation of the quasi-elastic proton direction with the virtual photon direction, given by BigBite on the electron arm, can also be measured directly and will test the assumptions made for the neutron case where the direction is obtained indirectly.

If a proton scattering asymmetry can be measured with reasonable precision, this will yield a value G_{Ep}/G_{Mp} from quasi-elastic $^2H(\vec{e}, e'\vec{p})$. If sufficient precision is obtainable, this can be compared to the free $p(e, e'p)$ case (E12-07-109). A more quantitative assessment of proton polarimetry capability is in progress.

With both sets of trackers in place, the separation of incident neutrons from protons will be extremely positive. This will rely not only on the production of signal in the GEM chambers, but also on the reconstructed hit position at the analyzer, as protons will be deflected vertically by the dipole.

The GEM detectors have initially been designed for the G_{Ep}/G_{Mp} experiment E12-07-109 which will run an 80 μA electron beam on a 40 cm hydrogen target. Thus they require to have a very high counting rate capability. Compared to E12-07-109, the present experiment will run at a factor ~ 8 lower luminosity and the polarimeter will sit at more backward angles. Thus we anticipate that the GEM chambers will operate comfortably in the present experiment. Detector rates are discussed in Sec.5.

3.2.3 The HCAL Hadron Calorimeter

Downstream of the tracker comes a 12×24 array of $15 \times 15 \times 90.8$ cm calorimeter modules (HCAL) which are formed from a stack of 80 alternating Fe and plastic scintillator plates. The total thickness of Fe is 50.8 cm and plastic scintillator 40 cm. HCAL will weigh around 40 tons and is under construction at CMU. Scintillation light is collected on a wavelength-shifting guide and then piped to a PMT. The time resolution for protons is expected to be $\sim$ 0.5 ns and a resolution of $\sim$ 0.3 ns has been measured for cosmic-ray muons. The response of HCAL to protons and neutrons will be very similar and detection efficiencies as high a 90% are expected, dependent somewhat on the applied energy threshold.

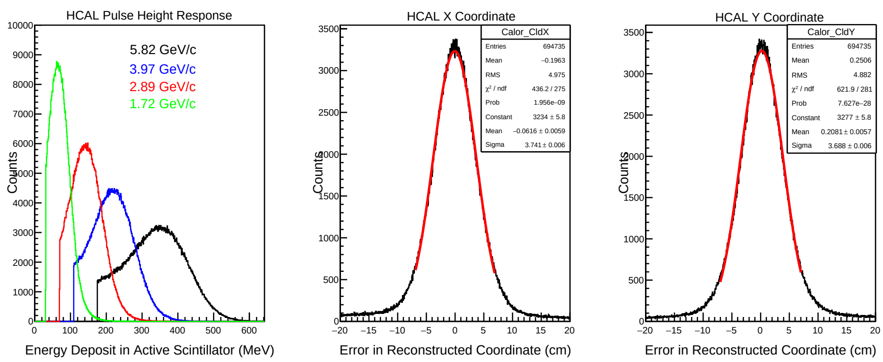

Figure 11: MC calculations of the HCAL response. **Left:** pulse height response for neutron momenta of 1.72, 2.89, 3.97 and 5.82 GeV/c; **middle:** the error in the reconstructed x-coordinate; **right:** the error in the reconstructed y-coordinate.

The simulated response of HCAL is displayed in Fig. 11 for neutrons incident on the polarimeter. Note that the Cu analyzer is in position so that HCAL is detecting both neutrons and protons. The peaked pulse-height response, resulting from the energy deposited in the scintillator sheets, enables thresholds to be set high to remove low energy background from the experimental trigger. The threshold cuts displayed in Fig. 11 correspond to half the peak channel of the distribution. With these cuts the percentage of incident nucleons that register a hit in HCAL is $\sim 70\%$.

The response has been calculated from an energy-weighted hit cluster analysis, which also gives a hit position. The differences between the reconstructed positions and the actual hit positions (recorded in the MC data stream) is displayed in the middle and right panels of Fig. 11. The widths (σ) of these distributions are$\sim$ 3.7 cm. Note that GEM chambers, rather than HCAL, will provide the primary information on the scattered proton direction. However the position sensitivity of HCAL will provide a useful correlation with the GEM track and the CDet position.

3.2.4 Rear Detector for Charged-Particle Identification

A "Coordinate Detector" (CDet) will sit immediately in front of HCAL to provide additional particle identification and hit coordinate information. It is under construction at JLab by Christopher Newport University (CNU) and is based on $0.5 \times 4.0 \times 51.0$ cm plastic scintillator strips arranged in modules of 392 elements. A total of 6 modules will give an area of 204×294 cm. Scintillation light produced in a strip is collected on a 2 mm diameter fast, wavelength shifting fiber and then transported to a multi-anode PMT. High-sensitivity front-end electronics, similar to those used on the GRINCH gas Cherenkov (Sec.3.1.3), will provide signals for recording of pulse charge and time. CDet is projected to have a coordinate resolution of 2 mm, a time resolution of 0.8 ns and a proton detection efficiency of 95%. It will also be used in the G_{Ep}/G_{Mp} experiment E12-07-109, the G_{En}/G_{Mn} experiment E12-09-016 and the G_{Mn}/G_{Mp}experiment E12-09-019. In the last two cases its placement, immediately in front of HCAL, will be identical to that proposed here.

3.2.5 Large-Angle Proton Detection

.

In addition to the primary goal of studying the charge-exchange channel for recoil polarimetry, there is also the potential to extract valuable information on the large-angle proton scattering channel. To this end, two active-analyzer, scintillator bars will be placed in vertical orientation near the left and right ends of the copper analyzer. The GEM planes before the analyzer will provide charged-particle identification for vetoing in software. Recoil protons emitted at large angles from n - p quasielastic scattering will be tracked by the GEM planes behind the analyzer and this tracking will be extended using additional GEM planes, placed in the shielded areas along the left and right edges, outside of the flux of primary neutrons produced in the target. Additional scintillator planes will be placed downstream of the GEMs, along the large-angle tracks in the left and right regions, shielded by the 48D48 yoke from direct view of the target. These will provide precise timing information.

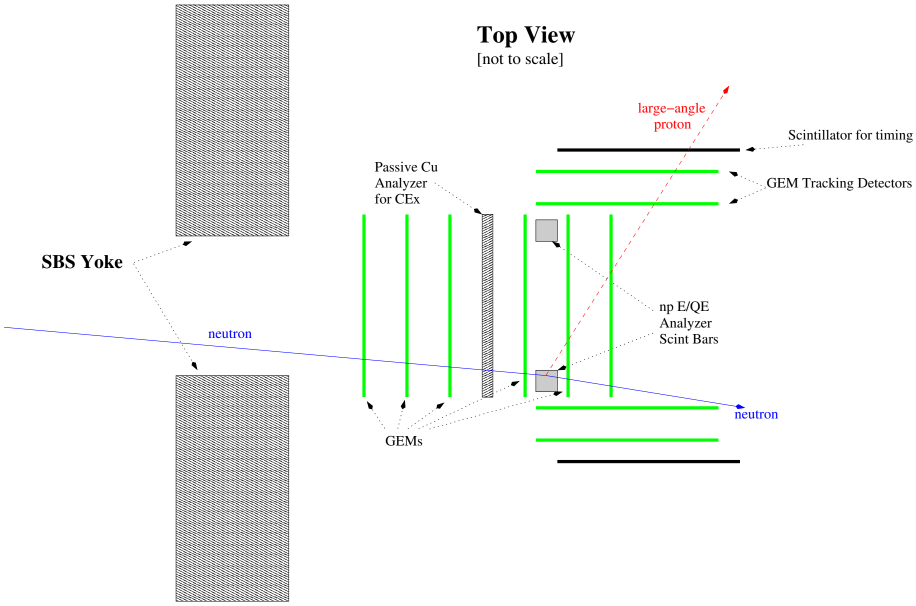

Figure 12: Preliminary schematic of the systems which enable large-angle proton detection within the SBS polarimeter.

Figure 12 shows a preliminary conceptual layout. Simulations of the acceptance and figure merit are being developed.

3.2.6 The 48D48 Dipole

For neutron polarimetry the dipole (known as 48D48) has no direct use as a spectrometer, but it serves several purposes:

1. To precess the longitudinal component of spin of the recoiling neutron to the vertical direction as the nucleon polarimeter measures transverse components of spin only.

2. To analyze the momenta of protons produced in quasi-elastic ^{2}H(e, e′p), which in principle can yield information on G_E^p/G_M^p derived in quasi-elastic scattering. Detection of the protons will also separate them from neutrons and further separation will be achieved through angular correlations (after proton deflection) with the $\vec{q}$ vector of the virtual photon, determined from the electron arm.

3. To sweep low-momentum, charged background out of the acceptance of the polarimeter. For an integrated field strength of 2 Tm, all charged particles with momenta below ∼1 GeV/c are swept beyond the acceptance of HCAL.

The dipole is currently being modified at JLab with new coils and a slot cut in the return yoke to provide space for the exit beam line when the spectrometer is moved to forward angles.

4 Monte Carlo Simulations of the Polarimeter

4.1 Neutron Spin Precession

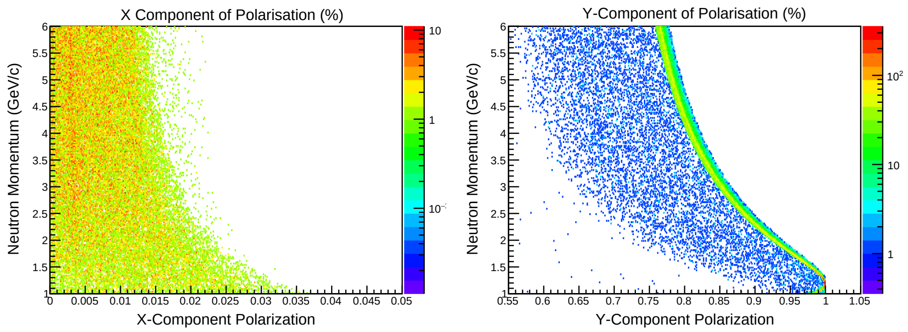

Figure 13: Neutron spin precession as a function of neutron momentum for an initial polarization (0,0,1). Left: induced values of P_x. Right: induced valued of P_y.

Neutron spin precession through the dipole field has been calculated using the Geant-4 polarimeter model. Non-perpendicular incidence with respect to the field direction, due to fringe fields and a finite angular range, produces small rotations in the $z-x$ plane which can distort the ratio P_x/P_z and hence $\mathrm{G_E/G_M}$. The 48D48 dipole, is currently being modified for use in Hall A, and thus a field measurement is not yet available. However, we have calculated the size of possible $z-x$ mixing effects using field maps obtained using the 3D code TOSCA [53]. The employed field map calculation did not include any field clamps and thus probably over estimates the amount of stray field, which extends beyond the confines of the dipole aperture. At a coil excitation of ~ 2000 A, an integrated field strength of ~ 1.7 Tm is calculated, which produces a spin rotation $z \rightarrow y$ (Fig.13). Neutrons with an initial polarization $\mathbf{P} = (0, 0, 1)$ and momenta of 1-6 GeV/c were tracked through the dipole field and their polarization recorded when they impinge on the analyzer. The value of P_x, calculated after the neutron has passed through the dipole, is at the few % level. P_y values range from ~ 1 at lower momenta, falling to ~ 0.75 at 6 MeV/c. Events off the main locus of the neutron momentum versus P_y curve are due to edge effects at the dipole aperture.

Fig.14 shows the variation of P_x and P_y over the incident coordinate at the analyzer at a neutron momentum of 3 GeV/c. Apart from events where the neutron is at the edge of the dipole aperture, P_x and P_y vary smoothly as a function of the hit position. If the maximum degree of spin transfer $z \rightarrow x$ is ~ 0.03 and the expected ratio P_x/P_z in a $\mathrm{G_E^n/G_M^n}$ measurement is ~ 0.2, then the maximum error induced in a measurement of P_x/P_z will be $\sim 15\%$. However given that the hit coordinate at the analyzer can be reconstructed to < 1 cm, and the maximum gradient $\delta P_x/\delta x$ is $\sim 0.002/cm$, the maximum error after correction will be $\sim 1\%$. The size of the effect, integrated over the angular acceptance of the SBS dipole, will be smaller.

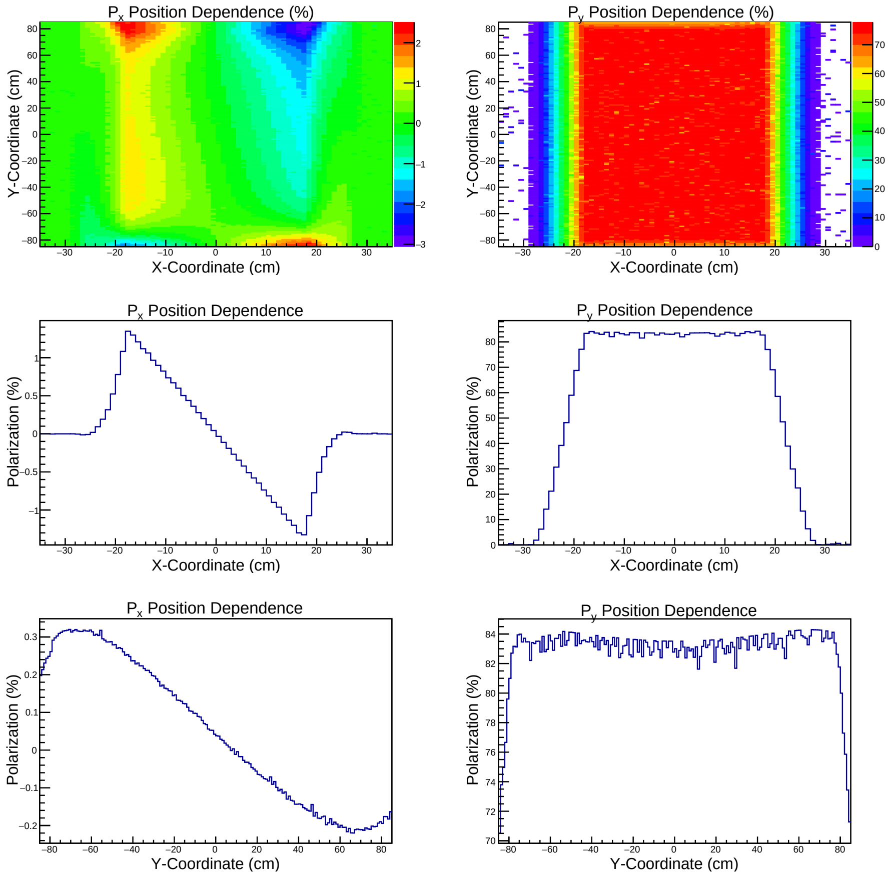

Figure 14: Neutron spin precession, variation with hit coordinate at front face of polarimeter

4.2 Separation of neutrons from protons

The present polarimeter will have a set of GEM trackers situated before the analyzer block, which will provide the primary identification and momentum analysis of protons produced in the target. Protons will be deflected by the 48D48 dipole, while neutrons will not, and correlation of the nucleon direction with the virtual photon direction given by the electron arm provides a secondary means of separation.

Fig. 15 displays the separation of the reconstructed out-of-plane (OOP) coordinate for neutrons and protons at the analyzer, after the protons have been deflected by the 2 Tm integrated field of the 48D48 dipole. The reconstruction procedure is described in Sec. 4.3. Equal numbers of 5.82 GeV/c neutrons and protons were incident on the analyzer, but the neutron signal is smaller as detection relies on CE $n-p$ scattering. The widths of the distributions arise dominantly from Fermi smearing of the quasi-elastic $d(e,e'N)$ process, but detector resolution effects are included. If a neutron-proton cut is set at an OOP position of 5 cm, then there is a 10% contamination of the neutron signal by

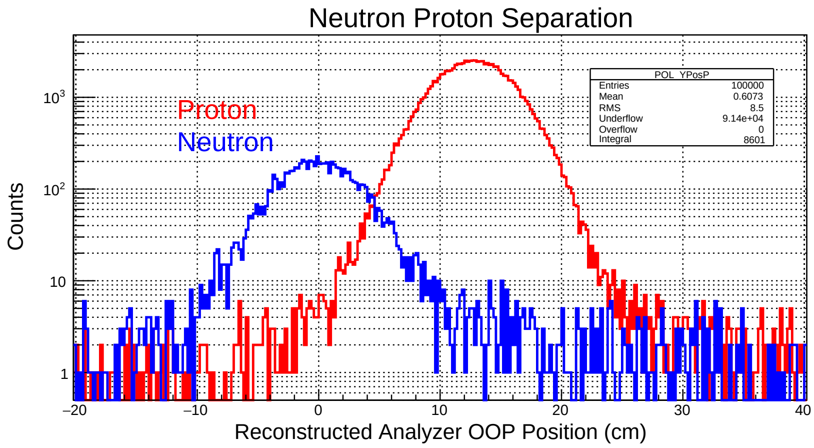

Figure 15: Separation of deflected and undeflected protons/neutrons at the Analyzer, reconstructed from the exit GEM trackers

protons. However protons will also be detected by the front set of GEM trackers. If this has an efficiency of 95% then the proton contamination of the neutron signal is reduced to $\sim 0.5\%$. At lower Q^2 kinematic settings, Fermi smearing will increase the widths of the distributions, but the lower momentum protons will be deflected by a larger amount so that the degree of overlap remains similar.

4.3 Polarimeter Angle Reconstruction

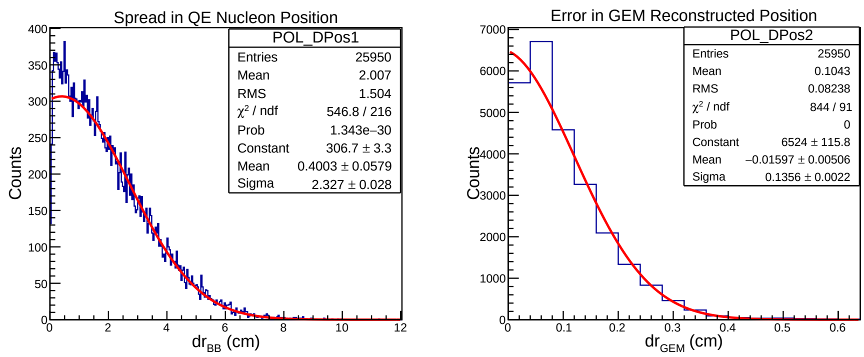

Figure 16: Reconstructed hit coordinate at the Analyzer at incident neutron momentum 5.82 GeV/c

Analysis of the polarimeter response involves reconstruction of the hits in the Analyzer and HCAL, followed by reconstruction of the polar and azimuthal components of the scattering angle. The scattering asymmetry is then obtained from $\sin\phi$ or $\cos\phi$ fits to the azimuthal distribution (Sec. 4.4). Any unpolarized variation in azimuthal acceptance is subtracted before the fit is made.

The present polarimeter is designed to detect protons produced after charge-

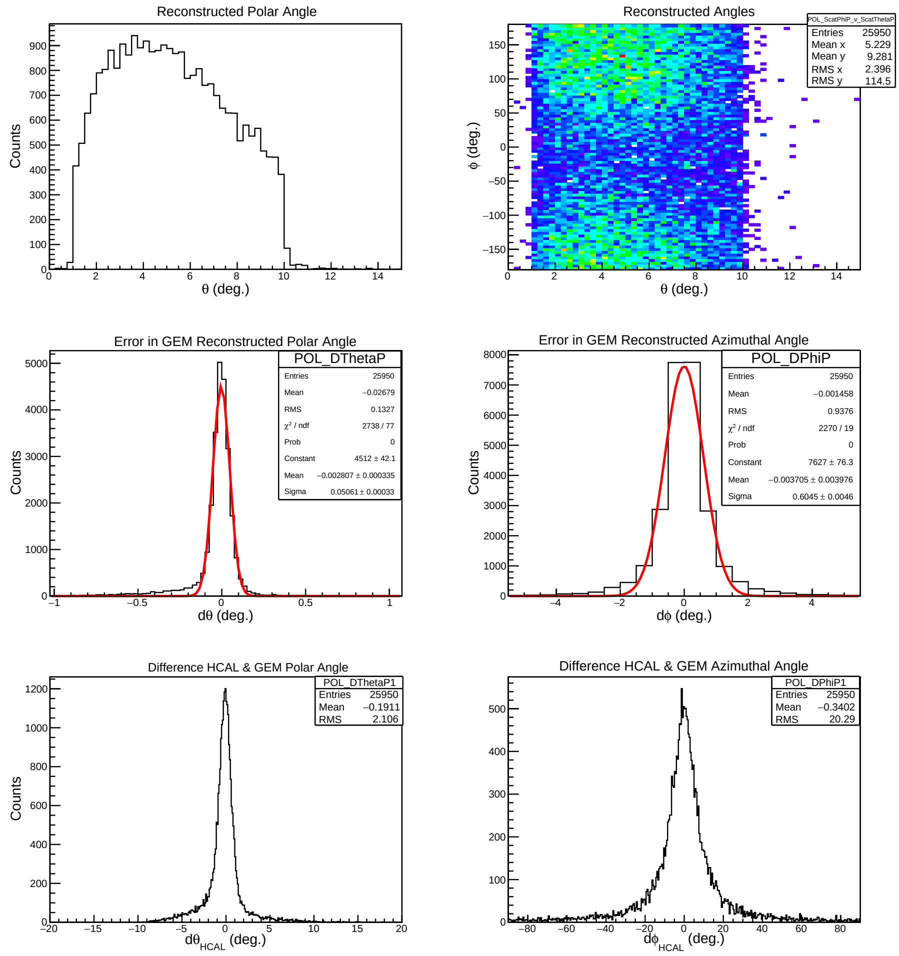

Figure 17: Polarimeter angle reconstruction at incident neutron momentum 5.82 GeV/c

exchange neutron scattering in the analyzer material. Quasi-elastic electron scattering from the deuteron will produce both protons and neutrons incident on the polarimeter, which will also detect $p-p$ scattering. The analyzer is inert so that the direction of the exiting proton is determined using the 3 GEM chambers situated after the analyzer (Fig.9). These have a coordinate resolution of ~ 0.07 mm. Additional position information is given by CDet, which sits immediately in front of HCAL, and has a coordinate resolution of ~ 2 mm. HCAL selects high momentum protons (Fig. 11) and has a coordinate resolution of ~ 4 cm so that a cluster of hits in the calorimeter modules can be correlated with a proton track.

Fig. 16 displays the reconstruction of the neutron interaction position at the Analyzer. The left panel shows the spread in position from that expected from the virtual photon direction given by BigBite. The spread is due mainly to the Fermi motion of the nucleon in the deuteron. The right panel shows the difference in position, projected on to the plane through the center of the analyzer, between the actual hit coordinate and that reconstructed from the GEM tracker. Fig. 17 displays the scattering angle reconstruction by the polarimeter for an incident neutron momentum of 5.82 GeV/c. The top panels show the polar and azimuthal angles reconstructed by the rear GEM tracker, while the middle panels display the difference between the actual and reconstructed angles. The bottom panels show the correlation between the GEM-track angle and the angle reconstructed from the hit coordinate in HCAL.

4.4 Determination of G_E^n/G_M^n from Simulated Azimuthal Asymmetries

The effects of finite size and imperfect reconstruction of the scattering process have been investigated using the polarimeter simulation. Multiple scattering in the analyzer effectively depolarizes the neutrons as the original reaction plane is lost, but the analyzer also requires to be sufficiently thick that a reasonable efficiency is maintained. New measurements from Dubna show that high values of analyzing power are obtained if the transverse momentum $P_t = P_N^{inc} \sin\theta_N \sim 0.2 - 0.85$ GeV/c so that optimum polar scattering angles fall in the range $2^\circ - 15^\circ$, dependent on incident momentum. The present geometry of the analyzer and GEM trackers produces a polar angle resolution of $\sim 0.05^\circ$ and azimuthal resolution of $\sim 0.6^\circ$ which is more than adequate.

Investigations have focused initially on dilution effects in the neutron polarimeter. For this the incident neutrons have been assigned $P_x = 0.19$ $P_y = 0.52$ which are typical of values expected, and the analyzing power set to 1 in order to obtain reasonable precision. Calculations have been made at incident momenta of 1.72 - 5.82 GeV/c, with the HCAL threshold set at 50% of the peak channel in the pulse-height distribution.

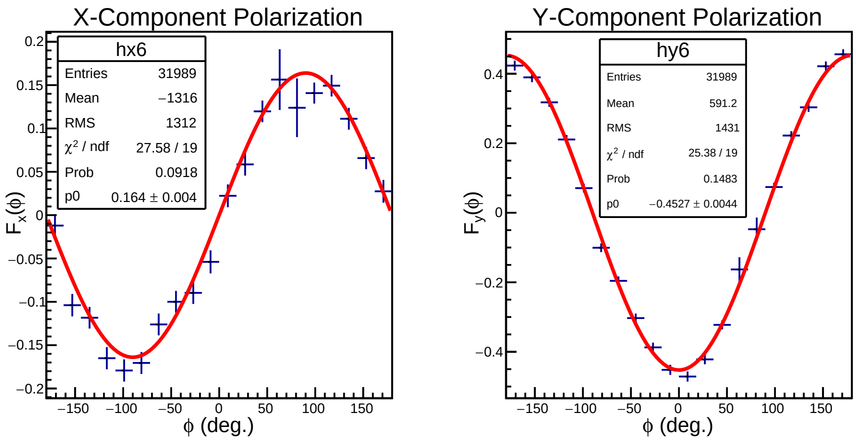

Figure 18: Simulated azimuthal distributions, Eq.15 at an incident neutron momentum of 3.15 GeV/c ($Q^2 = 4.5\ (\mathrm{GeV/c})^2$setting). The red curves are sine and cosine fits to $F_x(\phi)$ and $F_y(\phi)$ respectively.

The polarimeter will measure 4 combinations of the effective neutron polarizations in the x and y directions: $P_x^* = A_y^{eff} P_e P_x$ and $P_y^* = A_y^{eff} P_e P_z \sin\chi$, where A_y^{eff} is the effective analyzing power, $P_{x,z}$ are the x and z components of the recoil neutron polarization, P_e is the electron beam polarization (0.80) and χ is the angle of precession from $z \to y$ (Table6). With the azimuthal distribution described by

$$F(\phi_n^{'}) = C\{1 \pm |P_x^*| \sin\phi_n^{'} \pm \left|P_y^*\right| \cos\phi_n^{'}\}$$

then the four possible $\pm$ combinations are labeled F_{++}, F_{--}, F_{+-}, F_{-+} correspond to the four combinations of beam helicity flip ($P_{x,y}^* \to -P_{x,y}^*$) and the change of polarity of the 48D48 dipole ($P_y^* \to -P_y^*$). These may be used to separate the (relatively small) x component from the y. The unpolarized background and x, y components are given by:

$$\begin{aligned} C &= (F_{++} + F_{--} + F_{+-} + F_{-+}) \\ F_x &= (F_{++} - F_{-+} + F_{+-} - F_{--})/C \\ F_y &= (F_{++} - F_{+-} + F_{-+} - F_{--})/C \end{aligned} \tag{15}$$

$F_{x,y}$ are then fitted with sine and cosine functions to obtain the values of $P_{x,y}^*$ and their uncertainties $\delta P_{x,y}^*$. From this the estimated relative precision $\delta R/R$ of the ratio $R = \mathrm{G_E}/\mathrm{G_M}$ may be derived.

$$\frac{\delta R}{R} = \sqrt{\left(\frac{\delta P_x^*}{P_x^*}\right)^2 + \left(\frac{\delta P_y^*}{P_y^*}\right)^2} \tag{16}$$

p_n	A_y^x	A_y^y
1.72	0.91 ± 0.03	0.93 ± 0.01
2.89	0.91 ± 0.03	0.93 ± 0.01
3.15	0.86 ± 0.02	0.86 ± 0.01
3.97	0.92 ± 0.03	0.92 ± 0.01
5.82	0.85 ± 0.03	0.89 ± 0.01

Table 2: Effective polarimeter analyzing powers for x and y components of polarization at different incident neutron momentum p_n

Fig.18 shows simulated azimuthal scattering distributions made with $P_x^* = \pm 0.19$, $P_z^* = \pm 0.52$ and $A_y^{eff}(p_n, \theta_n^{'}) = 1.0$ calculated as described above. The incident momentum p_n was 3.15 GeV/c, corresponding to the $\mathrm{Q}^2 = 4.5$ (GeV/c)^2 kinematic setting, and the total number of incident neutrons simulated was 4×10^6. From the sine and cosine fits to F_x and F_y the effective analyzing power for the x-component is $A_y^x = 0.86 \pm 0.02$, while for the y-component it is $A_y^y = 0.86 \pm 0.01$. Table 2 shows the results for a range of incident neutron momenta. There seems to be no significant difference between x- and y-component analyzing powers, little significant dependence on incident momentum and the dilution factor of ~ 0.9 does not vary significantly with incident momentum.

The Dubna polarimeter covered a very similar angular range to the present device, used the same 4 cm Cu as an analyzer and employed almost identical calorimeter modules to select high-energy, forward-angle particles. We therefore assume that this polarimeter had a very similar dilution factor to the present one. This is already contained within the asymmetries measured at Dubna, and thus we have not applied any dilution correction.

Monte Carlo calculations have been performed, with a polarimeter analyzing power taken from a fit to the p_t dependence of the recent Dubna data. This checks that the precision in extracting polarization components, described above, is consistent with the simple estimate (Eq.12). Results are displayed in Fig.19. Scaling the amplitudes of the fitted asymmetries to the input polarizations (as above) the uncertainties in polarization are $\delta P_x = 0.0292$, $\delta P_y = 0.0291$. From Eq.11 and the FoM at 3.15 GeV/c (Fig. 8), $\delta P = 0.0295$ for 8×10^6 incident neutrons. The actual experiment proposes to collect 18×10^6 quasi-elastic neutrons at the equivalent setting $Q^2 = 4.5$ (GeV/c)^2 (Table 7).

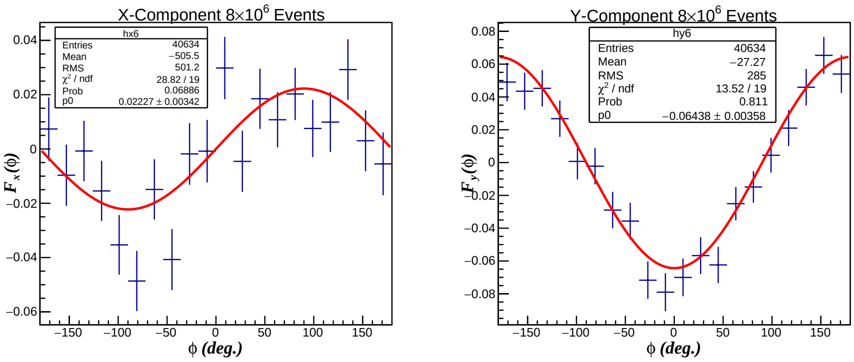

Figure 19: Distributions $F_x(\phi)$ and $F_y(\phi)$ (Eq.15) for $P_x = 0.19$, $P_y = 0.52$ for A_y taken from a fit to the Dubna asymmetry data.

Thus there is reasonable consistency to the procedure and Eq.11,12 provides a reasonable approximation when assessing necessary counting time.

4.5 Kinematics

Kinematic settings have been calculated for Q^2 = 4.5, 6.0, 9.3 (GeV/c)^2 and are summarized in Table 3. The nominal "central" values of the momenta and angles relate to free $n(e, e'n)$. Note that this proposal only concerns the $Q^2 = 4.5$(GeV/c)^2 point. Extractions at the larger Q^2 points are included to highlight the potential of exploiting the charge-exchange channel to reach the highest Q^2 values.

The ranges of kinematic variables for the nominal settings of the large acceptance detector system were calculated for quasi-free ^{2}H(e, e$'$n), where the internal momentum distribution of the neutron was sampled from $p_N^2 . \exp(-p_N^2/2\sigma_N^2)$, $\sigma_N = 0.03$ GeV/c, i.e. the Fermi momentum distribution was approximated by a Gaussian of width 0.03 GeV/c. Events were generated along the 10 cm length of the target and scattered electrons were detected within the effective 250×750 mm aperture of BigBite situated ~ 2 m from the target center. It was also checked if the recoiling neutron is within the acceptance of the 48D48

Setting	Q^2 (GeV/c)^2	E_e (GeV)	$p_{e'}$ (GeV)	θ_e (deg.)	θ_n (deg.)
1	4.5	4.4	2.01	41.9	24.7
2	6.0	6.6	3.40	30.0	25.0
3	9.3	8.8	3.81	30.7	19.4

Table 3: Kinematic Settings. Elastic n(e,e'n) central values. This proposal concerns the $Q^2 = 4.5(\mathrm{GeV/c})^2$ point only. The higher Q^2values are included to highlight the potential value of exploiting the charge exchange channel should this technique work as projected.

aperture. At the employed e' scattering angles, BigBite subtends a solid angle of 58.7 msr and in the worst case 87% of neutrons recoiling after quasi-elastic $^2H(e,e'n)$ pass through the aperture of the 48D48. The calculated $^2H(e,e'n)$ solid angle is given in Table 7. Fig. 20 (left) displays the calculated coverage in Q^2 while the BigBite angular acceptance and corresponding $^2\mathrm{H(e,e'n)}$ neutron acceptance are shown in Fig.20B - D for kinematic settings 1 - 3 of Table 3.

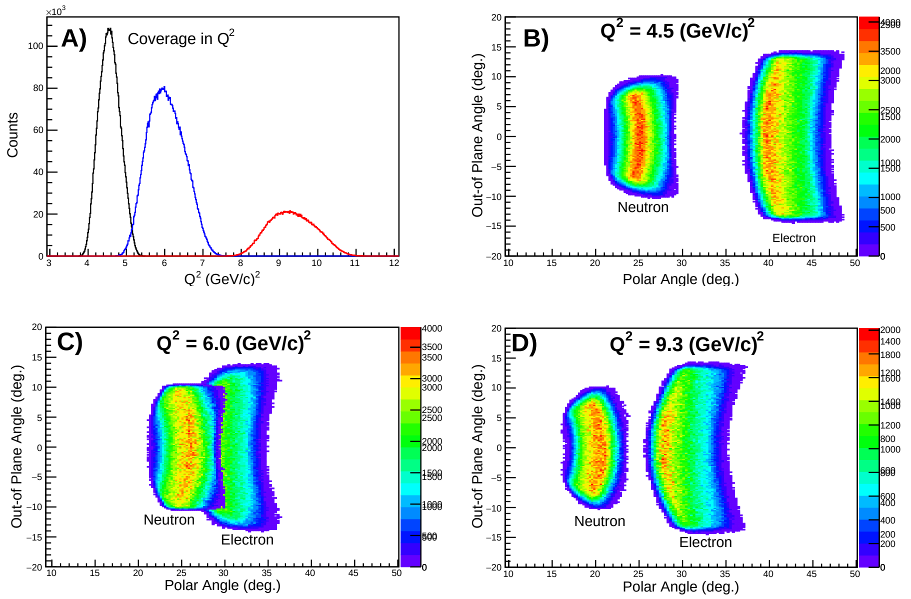

Figure 20: A) range of Q^2 for the nominal settings of Table 3. The distributions are weighted by the Mott cross section. B) electron/neutron angular coverage of BigBite/SBS at $Q^2 = 4.5$ (GeV/c)^2. [C) Angular coverage at $Q^2 = 6.0$ (GeV/c)^2. D) Angular coverage at $Q^2 = 9.3$ (GeV/c)^2].

4.6 Background Rates and the Trigger Rate

Detector rates have been evaluated using the SBS Monte Carlo simulation which models the detectors, magnets, the target and its vacuum chamber, beam lines and the concrete floor of Hall A. Two procedures have been used to generate events.

Tracking Plane	Rate (kHz/cm^2) 4.5 (GeV/c)^2
GEM-1	26
GEM-2	34
GEM-3	34
GEM-4	7
GEM-5	14
GEM-6	19
CDet-7	2.7 (420)

Table 4: Estimated average rates (kHz/cm^2) for tracking planes 1-7 of the polarimeter for the 4.5 (GeV/c)^2 kinematic setting. The calculation used procedure 1 (see text). GEM-1 is closest to the target. The figures in brackets give the average rate (kHz) in a $51 \times 3 \times 0.5$ cm plastic scintillator element of the CDet. These numbers

Kinematics	Procedure	Shower (kHz)	HCAL (kHz)	Coincidence (kHz)
4.5 (GeV/c)^2	1: G4	14	2200	1.54
4.5 (GeV/c)^2	2: EPC + G4	20	1700	1.70

Table 5: Trigger rates in the Shower and Hadron calorimeters and the Shower-Hadron coincidence rate within a 50 ns window. Procedure is explained in the text.

1. Geant4: electrons of a given beam energy are incident on the 10 cm LD_2 target and Geant-4 samples the interaction mechanism to produce final state particles. Interaction mechanisms included electromagnetic, low-energy electromagnetic, photo- and electro-nuclear, hadronic and high-precision (low-energy) hadronic particle.

2. QFS/EPC + Geant4: Inclusive cross sections, as a function of particle polar angle and momentum, were calculated using the QFS code for $e +^2 H \to e' + X$ and EPC code for $e +^2 H \to h$, where $h = p, n, \pi^0, \pi^-, \pi^+$. Both codes are described in Ref.[54]. The obtained 2D distributions of angle and momentum were then used to generate events randomly inside the LD_2 target volume, which were then tracked through the detector system by the Geant-4 simulation.

In both cases the output from the Monte Carlo simulation was analyzed to produce numbers of counts in detector elements as a function of applied energy threshold and these numbers were then scaled to an incident neutron luminosity of $1.25 \times 10^{38} s^{-1} cm^{-2}$.

Using procedure 1 a large number of events are necessary in order to generate a reasonable sample of background counts. It is useful to estimate backgrounds from low-energy electromagnetic processes and also low energy neutron processes. Soft electron/positron background from the target region is swept out of detector acceptance by the magnetic fields of the spectrometers, and much of the background registered by the GEM chambers is from soft photons. The

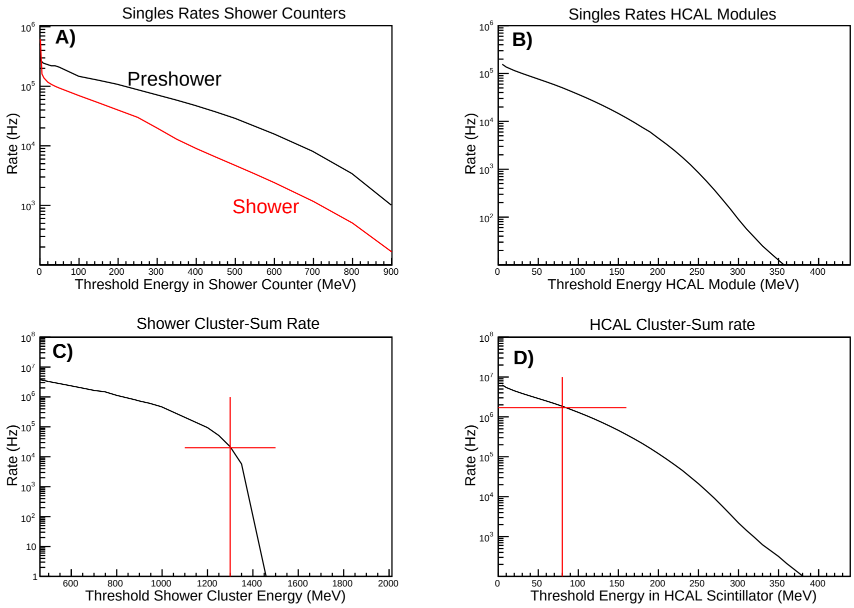

Figure 21: A) Singles rates in the BigBite Pb-Glass preshower and shower counters. B) Singles rates in the hadron calorimeter HCAL modules. C) Cluster-sum rates in the BigBite shower counters. The red cross shows the rate at an applied threshold of 1300 MeV. D) Hadron calorimeter cluster-sum rates. The red cross shows the rate at an applied threshold of 80 MeV. The calculation used procedure 2 (see text).

exit beamline also produces significant background and detailed studies are currently being made for the G_M^n/G_M^p experiment E12-09-019 to optimize shielding around the beam line.

Procedure 2 is faster and more useful for generating a reasonable sample of higher energy hadronic background, which has a greater bearing bearing on trigger rates in the BigBite electronmagnetic calorimeter and the hadron calorimeter HCAL, where cluster-summed energy thresholds are set high. The 48D48 field sweeps charged pions and protons below $\sim$ 1 GeV/c out of the acceptance of HCAL, but significant numbers of higher momentum charged particles, neutrons and photons from π^0 decay do interact.

Fig. 21 A,B displays the estimated singles rates, calculated using procedure 2, in elements of the BigBite electromagnetic calorimeter and the polarimeter hadron calorimeter. Table 4 gives the rates (in kHz/cm^2) of the GEM and CDet tracking detectors of the polarimeter calculated using procedure 1. The projected tracker rates, although substantial, are around an order of magnitude lower than expected for the G_E^p/G_M^p experiment. If the QE "spot" at the analyser for 4.5 (GeV/c)^2 kinematics has an area of $\sim 110\,cm^2$ the summed GEM-3 rate with that spot is $\sim$ 3.7 MHz. This translates to a $\sim$ 25% chance of an accidental hit within a coincidence resolving time of 50 ns.

The shower and hadron calorimeters are equipped with cluster-processing hardware such that a high threshold can be set on the cluster-summed energy to suppress background. Cluster rates as a function of applied threshold are displayed in Fig. 21 C,D for the electromagnetic and hadron calorimeters respectively. The red crosses denote the applied threshold levels, set at $0.65 \times E_{e'}$ for the Shower calorimeter and $0.5 \times E_{peak}$ (Fig. 11) for the Hadron calorimeter. The rates at these applied thresholds are listed in Table 5 and the numbers obtained using MC procedures 1 and 2 are reasonably consistent. Projected coincidence rates between the electron and hadron-arm calorimeters, within a 50 ns window, are well within the expected capability of the SBS DAQ system.

Should a further reduction in the raw trigger rate prove to be desirable, this will be possible via the GRINCH gas Cherenkov on the electron arm. According to the EPC calculation, around 95% of the shower trigger rate is due to photons produced by π^0 decay. Investigation of the inclusion of GRINCH signals into the trigger system is in progress.

4.7 Inelastic Background Rejection

With a front GEM tracker in position, its will be possible to separate quasi-elastic proton and neutron events cleanly. Inelastic processes, largely associated with pion electroproduction, constitute potential sources of background to the quasi-elastic ${}^2H(e,e'n)$ signal. Contamination of the electron-arm, quasi-elastic (QE) event sample by charged pions is expected to be extremely small due to the GRINCH gas Cherenkov in conjunction with PreShower-Shower pulse height correlation. The GRINCH will also be very effective at suppressing the photons from π^0 production. However the ${}^2H(e,e')$ signal will itself contain non-QE background which is estimated in the following, along with a simple but effective method of suppression.

It is expected that the present experiment, using a ^{2}H target will have significantly better separation of the QE signal than experiments which employ a ^{3}He target. The present experiment is similar in many respects to experiment E12-09-019 to measure $\mathrm{G_M^n}/\mathrm{G_M^p}$ [2], which also employs BigBite on the electron arm and the HCAL array on the nucleon arm. The momentum and angle resolutions are going to be the same on the electron arm and the angular resolution on the hadron arm will be better in the present case.

Modelling of the QE and background channels is based on the code QFS [54]. This phenomenological model gives a good account of inclusive (e,e') cross sections at incident energies of a few GeV and is used to generate the differential cross section $\sigma(\omega,\theta_q)$ for ${}^2H(e,e')$. Four reaction mechanisms have been considered: quasi-elastic scattering, quasi-deuteron absorption, resonance pion production (resonances at 1232, 1500, 1700 MeV) and deep inelastic scattering. The cross sections are then used in an event generator for a Monte Carlo procedure to calculate nucleon distributions after $\gamma^* + d \to n + X$. The angular acceptances of BigBite and the neutron polarimeter are included in the calculation. Fig. 22 shows calculated distributions of W^2 and θ_{qn}, where θ_{qn} is the angle between the virtual photon and the final-state neutron. Summed background includes pion electroproduction, quasi-deuteron absorption and deep inelastic scattering, with pion electroproduction via the $\Delta(1232)$ the dominant contributer. After application of a cut on W^2 and θ_{qn} (red box Fig. 22(Right)), 98.6% of the quasi elastic events survive and leakage of background events accounts for 1.5% of the quasi-elastic strength. The calculation includes the effects of BigBite angle and momentum resolution and the neutron polarimeter angle resolution, but these are small compared to the intrisic widths of the QE distributions.

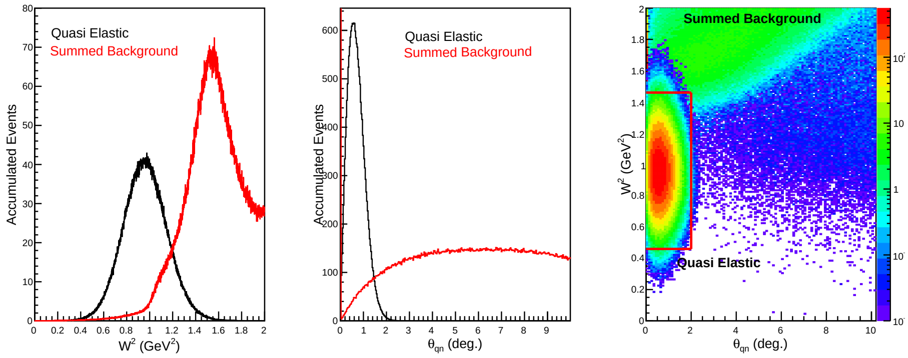

Figure 22: Separation of quasi-elastic and inelastic events for $d(e, e'n)$ events at $Q^2 = 4.5$ (GeV/c)^2. Left: separation in terms of W^2. Middle: separation in terms of θ_{qn}. The QE signal is in black, inelastic background in red. Right: W^2 vs. θ_{qn} distributions. Note that the z-scale is logarithmic. The red box shows the area used to select quasi elastic events.

4.8 Systematic Uncertainties

Potential sources of experimental systematic error are :

- The beam polarization is estimated as 80%, which affects the experimental precision, but the absolute value cancels in a ratio measurement. The electron beam helicity is flipped at a frequency of 30 Hz. The systematic uncertainty is assumed to be negligible.
- The analyzing power uncertainty cancels in a P_x/P_y ratio measurement, assuming it is the same for x and y components of neutron polarization. Polarimeter simulations (Sec. 4.4) do not show any significant variations and we estimate that the maximum size of an error of the ratio is $\sim 1\%$.
- Azimuthal angle acceptance non-uniformity, which should cancel after beam helicity flip and precession angle reversal (reversal of 48D48 field). Monte Carlo calculations are consistent with this and the precision of the calculation limits the size of a potential effect to a maximum of $\sim 1\%$.
- Separation of P_x from P_z does not rely on variation of the magnitude of the spin-precession magnetic field. In the present experiment P_x and $P_z (P_z \to P_y)$ are measured simultaneously with the same precession field, so that potential effects of changes to the background counting rates on the measured asymmetry are thus avoided. Non-uniformity of the magnetic field results in a small amount of $P_z \to P_x$ mixing. Given that the neutron interaction position at the analyzer can be reconstructed with good accuracy, the neutron path through the dipole can be reconstructed

accurately and this this effect corrected with an overall uncertainty of 1% (Sec. 4.1)

- Reproducibility of the spin precession angle after polarity reversal. At a precession angle of 60°, a 2% difference in integrated field would give 1% difference in rotated component $P_z \rightarrow P_y$. The 48D48 field strength will be monitored continuously during an experiment.
- Variation in the angle of spin precession through the dipole magnet. The path of a neutron through the dipole can be reconstructed with sufficient precision that a correction factor can be evaluated event by event. The estimated uncertainty is 0.25%.
- The vertical distribution of counting rates in the polarimeter will change when the polarity of the spin precession dipole is reversed. Any significant effect from changes to the level of signal contamination will show up when different combinations of beam-helicity-flip and dipole-flip asymmetries are compared.
- Dilution of the asymmetry by accidental background. The background is estimated to be at the 1% level (Sec.4.6) which can be subtracted without significant error.
- Contamination of the quasi-elastic signal by inelastic processes. Compared to ^3He, a deuteron measurement will have cleaner rejection of the inelastic background. An estimate of 1.5% is made (Sec. 4.7), based on Monte Carlo calculations of the amount of contamination of the QE signal by background processes.

Overall we estimate that a 3% systematic error or better is achievable.

5 Estimates of Experimental Precision

The estimate of experimental uncertainty in the ratio $R = G_E^n/G_M^n$ is based on the following:

1. The expected degree of polarization of the incident electrons. Previous measurements indicate that values in excess of 0.8 are generally available and we use the value 0.8 for the following estimates.
2. The acceptance of BigBite and the polarimeter for quasi elastic $^2\mathrm{H}(\mathrm{e}, \mathrm{e}'\mathrm{n})$. The kinematic settings are given in Sec.4.5.
3. The predicted detection efficiency and acceptance of the polarimeter is based on Monte Carlo simulations. The overall efficiency of the polarimeter, after scattering angle selection, is around 2-3%.
4. The analyzing power of n+Cu $\rightarrow$ p + X has been measured at JINR Dubna (Sec. 7) at a momentum of 3.75 GeV/c and the procedure to calculate the FoM for the proposed kinematic settings is described in Sec.2.2.1. The polarimeter figure of merit $\mathcal{F}^2$ has been obtained from a Monte Carlo evaluation of Eq.11, and the uncertainty in polarization from an asymmetry measurement from Eq.12.

5. The counting rate and polarization uncertainty estimate (Table 7) is based on a luminosity of $1.25 \times 10^{38}\ s^{-1}cm^{-2}$ per nucleon and the cross section and polarization for free $\mathrm{n(e,e'n)}$ scattering. Estimates of elastic cross section and polarization use the Galster [56] parametrization for G_E^n and the Kelly parametrization for G_M^n [57]. The dependence of the estimated precision on the assumed parametrization is very weak.

Q^2 $(\mathrm{GeV/c})^2$	p_n^{lab} GeV/c	P_eP_x	P_eP_z	$\mathcal{F}^2$ $\times 10^{-4}$
4.5	3.15	0.082	0.636	2.53
6.0	3.97	0.071	0.555	2.53
9.3	5.82	0.067	0.609	3.08

Table 6: Mean values of projected polarization parameters for the proposed measurement at 4.5 $(\mathrm{GeV/c})^2$. Values at the higher Q^2 points are included to hightlight the projected potential of this reaction channel in any future high-Q^2 G_E^n experiment.

Q^2 $(\mathrm{GeV/c})^2$	$\Omega_{e',n}$ (msr)	$\sigma_n(\theta)$ (pb/sr)	Rate (Hz)	Time (hr)	δP $\times 10^{-3}$	δR (stat)	(sys)
4.5	57.4	6.74	48.8	100	19.4	0.078	0.01
6.0	50.8	4.06	26.0	150	23.7	0.12	0.01
9.3	57.6	0.40	2.94	750	28.6	0.17	0.01

Table 7: Counting rate and error estimate for $^2H(\overrightarrow{e},e'\overrightarrow{n})$ at an incident (neutron) luminosity of 1.26×10^{38} $\mathrm{cm^{-2}s^{-1}}$. "Rate" is the mean $n(e,e'n)$ rate incident on the analyzer, δP is the statistical uncertainty in the polarization, δR (stat) is the statistical uncertainty in the ratio $R = G_E^n/G_M^n$ and δR (sys) is the systematic uncertainty (3% of R). As before, values at the two higher Q^2 points are included to hightlight the projected potential of this reaction channel in any future high-Q^2 G_E^n experiment.

Table 6 displays parameters relevant to the precision of the polarization measurement for neutron momenta (p_n^{lab}) associated with the present kinematic settings (Table 3). Table 7 gives estimates of the counting rate and projected precisions for the polarization δP and the ratio δR, $R = G_E^n/G_M^n$. The projected systematic uncertainty is also given, but this is small in comparison to the statistical uncertainty.

6 Beam Time Request

Beam time is requested (Table 9) to measure $\mathrm{G_E^n/G_M^n}$ at one value of Q^2. Electron beam helicity flip is performed at 30 Hz, so that combination with the up-down polarized data along with positive and negative field settings on the neutron polarimeter dipole will yield the effectively unpolarized azimuthal distributions in the polarimeter.

At each Q^2 point we will measure at two equal, but opposite polarity setting of the spin-precession dipole. This will effectively reverse the P_y (precessed from

P_z), to make the separation procedure of x and z (precessed to y) components of the recoil-neutron polarization more robust and provide an extra check on possible instrumental effects.

In order to determine the four-momentum of the virtual photon to best accuracy, the optics of BigBite has to be well known. We propose to use the calibrations made for E12-09-019 at an identical kinematic setting. Data will be taken with a multi-foil carbon target and a removable sieve slit of lead, located at the front face of the magnet. These provide the means to calibrate accurately the angular coordinates before magnetic deflection and also the scattering vertex position. The momentum calibration is obtained from elastic $e-p$ scattering from a LH_2 target, where the kinematics are very similar to the quasi-elastic $e-n$ case, so that detectors do not require to be moved.

6.0.1 $Q^2 = 4.5$ (GeV/c)^2

The beam time request is for a single kinematic point. The kinematics for the $Q^2 = 4.5$ (GeV/c)^2 setting has been chosen to be identical to that employed for the G_M^n/G_M^p experiment E12-09-019, which is scheduled to be the first SBS experiment to run in Hall A. Apart from the neutron polarimeter, the present experiment uses identical apparatus to E12-09-019 so that BigBite and HCAL settings could be reused without change. Calibration runs made for E12-09-019 could also be reused. The components of the polarimeter will be designed to be moved quickly in and out of the acceptance of the hadron arm and could be pre-prepared before the start of E12-09-019 for fast insertion after a cross section measurement at $Q^2 = 4.5$ (GeV/c)^2 has taken place. Thus a modest extension of 96 hr production running and 12 hr setup to the E12-09-019 beam time would yield a data point for G_E^n/G_M^n which extends the Q^2 range of world data from 3.4 (GeV/c)^2 to 4.5 (GeV/c)^2. It would also serve as a check that the projections of the experimental uncertainties are accurate, before additional beam time is scheduled. A break down of the requested time is given in Table 8

Q^2	Function	Target	Precession	Time (hr)
	Insert Polarimeter into E12–09-019 setup			12
4.5	Production$^2H(\vec{e}, e'\vec{n})$	LD_2	pos	48
4.5	Production$^2H(\vec{e}, e'\vec{n})$	LD_2	neg	48
4.5	Use E12-09-019 BB optics calibration	C Foil		0
4.5	Use E12-09-019 momentum calibration	LH_2		0
Total				108

Table 8: Breakdown of Beam Time Request

6.0.2 $Q^2 = 6.0,\ 9.3$ (GeV/c)^2

We include an estimate of the beam time necessary to measure G_E^n/G_M^n by charge-exchange neutron scattering at the the kinematic settings $Q^2 = 6.0, 9.3$ (GeV/c)^2. At this stage **we do not request time** for these points, but propose to return to the PAC once the performance of this approach has been verified at $Q^2 = 4.5$ (GeV/c)^2 .

The kinematic points have been chosen to maximize the experimental counting rate and are somewhat different to those proposed for E12-09-019. However whatever the design of the experiment, a dedicated measurement will be necessary to achieve high Q^2. Due to the rapidly falling cross section, high Q^2 requires more production time to achieve a precision with the power to discriminate between theoretical models. An estimate of the beam-time breakdown of a charge-exchange experiment is given in Table 9. BigBite optics and momentum calibrations would be necessary at each point, as well as time to move the spectrometers to new angles. In total these data points would require 900 hr of production running, 120 hr for calibrations with beam and 12 hr for a configuration change.

Q^2	Function	Target	Precession	Time (hr)
6.0	Production$^2H(\vec{e}, e'\vec{n})$	LD_2	pos	75
6.0	Production$^2H(\vec{e}, e'\vec{n})$	LD_2	neg	75
6.0	BB Optics etc.	C Foil		24
6.0	^{1}H$(e, e'p)$	LH_2		24
	Angle Change			12
9.3	Production$^2H(\vec{e}, e'\vec{n})$	LD_2	pos	375
9.3	Production$^2H(\vec{e}, e'\vec{n})$	LD_2	neg	375
9.3	BB Optics etc.	C Foil		24
9.3	^{1}H$(e, e'p)$	LH_2		48
Total				1032

Table 9: Breakdown of beam time estimate for potential future kinematic points

7 Summary and Comparison with other G_E^n/G_M^n measurements at Jefferson Lab.

We propose to measure the ratio $\mathrm{G_E^n/G_M^n}$ from a double-polarization asymmetry, using the longitudinally polarized CEBAF electron beam and a polarimeter to measure the transfer of polarization to the recoiling neutron in quasi-elastic ^{2}H$(\vec{e}, e'\vec{n})$. The measurement will be made at one value of the squared four-momentum transfer of the scattered electron: $Q^2 = 4.5$ (GeV/c)^2. This data point will not only provide highest Q^2 G_E^n/G_M^n measurement worldwide, but also provide vital data for future experiments at higher Q^2. With these future data points the unknown behavior of $\mathrm{G_E^n/G_M^n}$ at moderate Q^2 will be determined, thus discriminating between the very different behaviors (Fig. 23) predicted by different nucleon-structure models. In particular they will show if the ratio bends over and heads towards zero with increasing Q^2, as predicted by recent DSE calculations or continues to increase with increasing Q^2. Since the availability of G_E^n data determines the Q^2 range over which $u - d$ flavor separation of $F_1(Q^2)$ and $F_2(Q^2)$ is possible, the present and future data would also result in a large extension in range. With present data, separation is only possible up to 3.4 (GeV/c)^2.

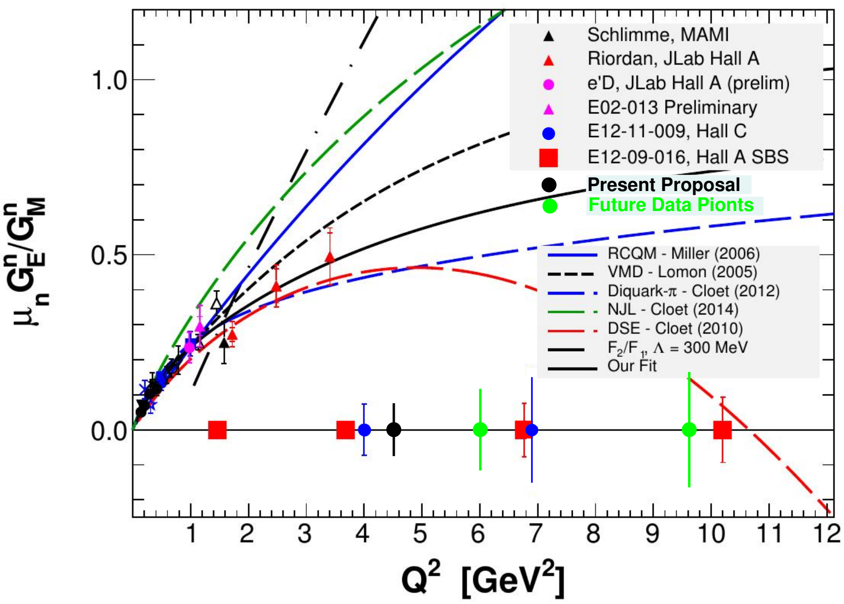

Figure 23: A comparison of the uncertainties of this proposal (black circles) with those of E12-09-016 [1] (red squares) andE12-11-009 (blue circles). The green data points reflect projected uncertainties for a future extended run with the SBS apparatus (Sec. 6.0.2). The blue data points reflect the E12-11-009 (C-GEN) proposal projections that did not include sensitivity to the charge-exchange channel under study here. Data from the proposed measurement will be used to study extensions to the C-GEN polarimeter to enhance its sensitivity to this reaction channel.

The employed apparatus will mainly use components already under construction for other SBS EMFF experiments and will closely resemble that of E12-09-019 to measure G_M^n/G_M^p. In particular it will employ the same target, electron arm and calorimeter on the hadron arm. On the hadron arm, a neutron polarimeter will be constructed by introducing GEM tracking components from E12-07-109 to measure G_E^p/G_M^p, a Cu block of analyzing material and components to provide sensitivity to large-angle protons. Thus the polarimeter will measure asymmetries produced by $\vec{n}+Cu \to p+X$, $\vec{n}+X \to p+X$, as well as $\vec{p}+Cu \to p+X$ from quasi-elastic $^2\mathrm{H}(\vec{e},e^{'}\vec{p})$. This novel approach has been inspired by new analyzing power data from JINR Dubna on polarized, charge-exchange scattering at $p_N \sim 4$ GeV/c. Preliminary analyses of these data show sizable values of the analyzing power..

This experiment will provide critical data to validate the charge-exchange channel as an effective method for recoil polarimetry. It will probe the sensitivity and identify challenges associated with this technique, allowing the determination of an optimal approach to executing a long run at high Q^2 in the future. Options to be considered include pursuing the measurement within the SBS configuration in Hall A, through to an enhanced version of the C-GEN design in Hall C, or a combined approach staged in either Hall.

The Collaboration

Not yet finalized

This experiment will be performed in Hall-A of Jefferson Laboratory. It will be part of the SBS program of experiments and the bulk of the necessary major apparatus (BigBite, the SBS dipole, HCAL, the GEM tracking systems and the Coordinate Detector) will be used in other experiments. The joint international effort encompasses groups from the USA (JLab, UVa, CMU, W&M, CSU, CNU, NSU, ISU, NCAT), the UK (Glasgow), Italy (INFN Catania and Rome), The Russian Federation (JINR Dubna) and Canada (St. Mary's).

We list the institutes which have been involved in building the apparatus required by the present experiment .

- **Jefferson Laboratory (JLab):**
  JLab supervise the entire SBS programme of experiments. They are responsible for the design of the apparatus mechanical structures, the modification of the 48D48 magnet and beam-line vacuum pipe. They will supervise the installation and commissioning of the upgraded infrastructure required for the magnet, the targets, the beam line and the BigBite electron spectrometer. JLab have negotiated with SLAC the transfer of 6000 photomultipliers (originally used for BaBar) for use in BigBite and the SBS.

- **University of Glasgow (UGla):**
  UGla have initiated R&D on the polarimeter, have a Ph.D. student working on this investigation and have participated in the polarized neutron measurements at JINR Dubna. They are responsible for the new BigBite timing hodoscope and the front-end amplifier/discriminator electronics used in the GRINCH, Hodoscope, CDet and HCAL, comprising several thousand channels.

- **JINR Dubna (JINR):**
  JINR lead the effort to measure the analyzing power of polarized neutron and proton scattering from various materials (CH_2, CH, C, Cu) at neutron momenta of several GeV/c. This uses the polarized nucleon beams, derived from polarized deuterons produced by the Nuklotron accelerator in JINR. They have ensured the necessary provision of beam, apparatus and subsistence for foreign researchers to carry out the measurement.

- **INFN Catania (CATANIA):**
  CATANIA have made large contributions to HCAL, and electronics for HCAL and CDet

- **INFN Rome Sanita (ROME):**
  ROME lead the effort to build the high-resolution, front tracker GEM chambers, used in BigBite, and also the design and implementation of the GEM readout electronics based on the APV25 chip. These detectors also form the forward trackers of the SBS proton polarimeter and will benefit all experiments which use the common apparatus.

- **University of Virginia (UVa):**
  UVA group lead the effort to build the large rear GEM chambers, used

in the polarimeter and BigBite, and are also heavily engaged in chamber R&D work. These detectors also form the rear trackers of the SBS proton polarimeter, as well as the extended tracking system to detect large-angle recoiling protons, and will benefit all experiments which use the common apparatus.

- **Carnegie Mellon University (CMU):**
  CMU group lead the construction effort on the hadron calorimeter modules. They have optimized the pulse height response and time resolution. HCAL will be the high efficiency nucleon detector for several SBS experiments and will benefit all experiments which use the common apparatus.

- **College of William and Mary (W&M)**:
  W&M are responsible for the GRINCH gas Cherenkov detector for BigBite, which will provide more selective triggering on electrons, as well as improved $e^- - \pi^-$ separation. This work will benefit all experiments which use BigBite.

- **Christopher Newport University (CNU):**
  CNU have taken over responsibility for the assembly and testing of modules for the Coordinate Detector, which will sit before the hadron calorimeter and provide charged particle identification and vetoing capability. This detector is being designed initially for the electron arm of the GEp(5) experiment, but it is also suitable for use with HCAL and will benefit all experiments which use the common apparatus.

- **Hampton University (HU)**
  HU have experience with GEM detectors and APV+MPD readout electronics from their involvements in OLYMPUS, MUSE and DarkLight. HU is located in close proximity to JLab; the group will join the testing, commissioning and installation effort of the GEM modules onsite at Jefferson Lab.

- **Idaho State University (ISU)**
  ISU have made a large contribution to the development of the coordinate detector.

- **North Carolina A&T (NCAT)**
  NCAT are actively engaged in the testing and construction of components of the SBS system

- **St. Mary's University (SMU):**
  SMU have provided significant contribution to development of the coordinate detector, notably testing multianode PMTs.

- **James Madison University (JMU)**
  JMU have provided effort for testing of photomultipliers used in the GRINCH gas cherenkov and other detectors used for SBS experiments.

- **California State University (CSU)**:
  CSU have manufactured PMT housings for the BigBite timing hodoscope, which exclude He from the PMT.

Cost Estimate of New Components

All of the detectors used in this experiment will be built for previously approved SBS experiments in Hall A and so there will be no additional cost on that side. A Cu analyser block is estimated to cost $5000-10000 and possible mechanical modification to polarimeter mounting platforms could be in the region $10000.

Cost of additional scintillation counters for polarimeter?

Appendix A. Measurement of Neutron and Proton Analyzing Power at JINR Dubna

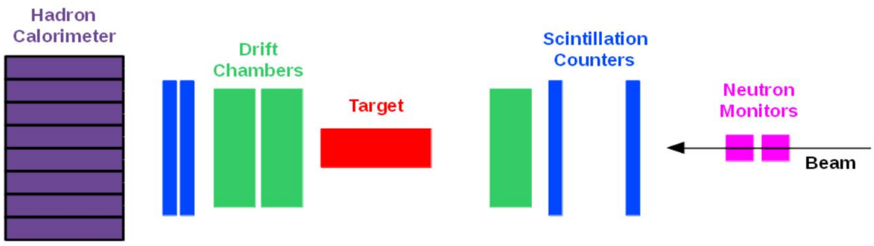

Figure 24: Representative schematic (not to scale) of the Dubna polarimeter. The target is the analyzer material under investigation.

The Dubna experiment [?] measures analyzing powers for different materials using polarized neutrons with momentum (p_n) up to 4.5 GeV/c and polarized protons with momentum (p_p) up to 7.5 GeV/c [58] . This provides entirely new neutron information for $n{+}Target \rightarrow p{+}X$ and extends previous proton results for $p{+}CH_2 \rightarrow p{+}X$ at $p_p = 1.75 - 5.3$ GeV/c [59]. These data are vital for SBS measurements of G_E^n/G_M^n and G_E^p/G_M^p. The data were collected in November 2016 and February 2017.

Neutrons or protons were derived from the breakup of polarized deuterons striking a Be target, separated by means of a dipole magnet and then collimated. An ionization chamber was used to estimate proton intensities and a polarimeter, comprising several scintillation counters located around the proton target, was used to give a measurement of the deuteron beam polarization. For neutrons, a monitoring system consisting of CH_2 elements and scintillation counters was installed after the collimator.

The nucleon polarimeter (Fig. 24) consisted of scintillation counters for triggering, a series of drift chambers for charged particle tracking and a segmented hadron calorimeter for the detection of final state particles. Several different analyzing materials were used, including: 30 cm CH_2; 20 cm C; 4 cm Cu, and active CH scintillator.

Online analysis of neutron data taken in Feb. 2017 indicated that a Cu target has a similar analyzing power to C and produced a factor $\sim$ 3 increase in the detected yield of protons. Inclusion of hadron calorimeter cuts, to remove events with large scattering angle and low pulse height, increased the obtained asymmetries. Pending confirmation of the preliminary analyses, we are not at liberty to release any analyzing power information, but this has been used in constructing the polarimeter FoM (Sec. 2.2.3) for the present proposal.

References

[1] *Measurement of the Neutron Electromagnetic Form Factor Ratio* $\mathrm{G_E^n/G_M^n}$ *at High* Q^2, JLab Experiment E12-09-016, Spokespersons: G. Cates, S. Riordan, B. Wojtsekhowski. *The Electric Form Factor of the Neutron with SBS*, S. Riordan, SBS Review, March 28, 2012.

[2] *Precision Measurement of the Neutron Magnetic Form Factor at to* $\mathrm{Q}^2 = 18$ (GeV/c)^2. Jefferson Lab experiment E12-09-019, Spokespersons: J. Annand, R. Gilman, B. Quinn, B. Wojtsekhowski,

[3] *Large Acceptance Proton Form Factor Ratio Measurements at 13 and 15* (GeV/c)^2 *Using Recoil Polarization Method,* JLab Experiment E12-07-109, Spokespersons: E. Cisbani, M. Khandaker, C.F. Perdrisat, L.P. Pentchev, V. Punjabi, B. Wojtsekhowski.

[4] *Precision Measurement of the Proton Elastic Cross Section at High* Q^2, JLab. experiment E12-07-108, Spokespersons: J. Arrington, S. Gilad, B. Moffit, B. Wojtsekhowski.

[5] *The Neutron Electric Form Factor at* Q^2 *up to* 7 (GeV/c)^2 *from the reaction* $^2\mathrm{H}(\vec{e},\mathrm{e}'\vec{n})$ *via Recoil Polarimetry.* JLab. Experiment E12-11-009, Spokespersons: B.D. Anderson, J. Arrington, S. Kowalski, R. Madey, B. Plaster, A. Yu. Semenov. *E12-11-009 (G_{En}) Update,* M. Kohl, Hall C Users Meeting, Feb. 21-22, 2014.

[6] S. Riordan *et al.*, Jefferson Lab experiment E02-013, Phys. Rev. Lett. 105(2010), 262302.

[7] B. Plaster *et al.,* Phys. Rev. C73(2006), 025205., R. Madey *et al.*, Phys. Rev. Lett. 91(2003),122002.

[8] S.J. Brodsky, G.R. Farrar, Phys. Rev. D11(1975), 1309.

[9] M.K. Jones *et al.* Phys. Rev. Lett. 84(2000), 1398.

[10] O. Gayou *et al.*, Phys. Rev. Lett. 88(2002), 092301.

[11] V. Punjabi *et al.*, Phys. Rev. C71(2005), 055202.

[12] A.J.R. Puckett *et al.,* Phys. Rev. Lett. 104(2010), 242301.

[13] A. Puckett et al., Phys. Rev. C85(2012),045203.

[14] L. Andivahis *et al.*, Phys. Rev. D50(1994), 5491.

[15] M.E. Christy *et al.*, Phys. Rev. C70(2004), 015206.

[16] I.A. Qatten *et al.*, Phys.Rev.Lett. 94(2005), 142301.

[17] G.D. Cates, C.W. De Jager, S. Riordan and B. Wojtsekhowski, Phys. Rev. Lett. 106(2011), 252003.

[18] J. Koponen et al, arXiv:1701.04250v1, 16 Jan. 2017

[19] C.D. Roberts and A. G. Williams, Prog. Part. Nucl. Phys. 33(1994), 477.

[20] I.C. Cloët *et al.*, Few-Body Syst., 46 (2009), 1.

[21] J. Segovia *et al.*, Few-Body Syst. 55 (2014), 1185.

[22] D.J. Wilson *et al.*, Phys. Rev. C85(2012),025205.

[23] I.Cloet et al., Phys. Rev. C 90, (2014), 045202.

[24] R. S. Sufian et al., Phys. Rev. D95(2017),014011.

[25] I. A. Qattan and J. Arrington, Phys. Rev. C86(2012),065210.

[26] M.Diehl and P.Kroll, Eur. J. Phys. C73 (2013), 2397.

[27] I. Passchier *et al.*, Phys. Rev. Lett. 82(1999), 4988.

[28] H. Zhu. Phys. Rev. Lett. 87(2001), 081801.

[29] G. Warren *et al.*, Phys. Rev. Lett. 92(2004), 042301.

[30] M. Meyerhoff *et al.* , Phys. Lett. B 327(1994) , 201.

[31] J.Becker *et al.*, Eur. J. Phys. A6(1999), 329.

[32] D.Rohe *et al.*, Phys. Rev. Lett. 83(1999), 4257.

[33] B.S. Schlimme, Proc. SPIN2010, J. Phys.: Conf. Ser. 295 (2011), 012108.

[34] T. Eden *et al.*, Phys. Rev. C50(1994), 1749.

[35] C. Herberg *et al.*, Eur. J. Phys. A5(1999), 131.

[36] M. Ostrick *et al.*, Phys. Rev. Lett. 83(1999), 276.

[37] D.I. Glazier *et al.*, Eur. J. Phys. A24(2005), 101.

[38] *Measurement of the Neutron Magnetic Form Factor at High Q2 Using the Ratio Method on Deuterium* , JLab. Experiment E12-07-104, Spokespersons: G.P. Gilfoyle, W.K. Brooks, M.F. Vineyard, J.D. Lachniet, L.B. Weinstein, K. Hafidi.

[39] A.I. Akhiezer *et al.*, JEPT 33(1957), 765.

[40] R.G. Arnold *et al.*, Phys. Rev. C23(1981), 36.

[41] M. M. Sargsian *et al.*, Phys. Rev. C 71(2005), 044614.

[42] N.V. Vlasov *et al.*, Instr. and Exp. Tech. 49(2006), 49.

[43] R. Diebold *et al.*, Phys. Rev. Lett. 35(1975), 632.

[44] S.L. Kramer *et al.*, Phys. Rev. D17(1978), 1709.

[45] H. Spinka *et al.*, Nucl. Instr. and Meth. A211(1983), 239.

[46] L.S. Azhgirey *et al.*, Nucl. Instr. and Meth. A538(2005), 431.

[47] N.E. Cheung *et al.*, Nucl. Instr. and Meth. A363(1995), 561.

[48] I.G. Alekseev *et al.*, Nucl. Instr. and Meth. A434(1999), 254.

[49] P.R. Robrish et al., Phys. Lett. B31 (1970), 617.

[50] M.A. Abolins et al., Phys. Rev. Lett. 30 (1973), 1183.

[51] *Measurement of analyzing powers for the reaction* $p + CH_2$ *up to 7.5 GeV/c and* $n + CH$ *up to 4.5 GeV/c at the Nuclotron,* ALPOM2 proposal to JINR Dubna PAC, March 2015, Spokespersons: N.M. Piskunov, C.F. Pedrisat, V. Punjabi, E. Tomasi-Gustafsson.

[52] *Analyzing Power of pp and np Elastic Scattering at Momenta between 2000 and 6000 GeV/c and Polarimetry at LHE*, V.P. Ladygin, JINR report E13-99-123, 1999.

[53] TOSCA/Opera-3D, Vector Fields Software, Cobham Technical Services, Dorset, UK

[54] J. W. Lightbody and J. S. O'Connell, Computers in Physics 2(1988),57; http://dx.doi.org/10.1063/1.168298

[55] P.V. Degtyarenko, computer code DINREG, *Applications of the Photonuclear Fragmentation Model to Radiation Protection Problems*, Proc. Second Specialist Meeting on Shielding Aspects of Accelerators (SATIF2), CERN, October 1995.

[56] S. Galster *et al.*, Nucl. Phys. B32 (1971), 221.

[57] J. J. Kelly, Phys. Rev. C70(2004), 068202.

[58] N.M. Piskunov et al., Physics of Particles and Nuclei, 2014, Vol. 45, No. 1, pp. 330–332.

[59] I.M. Sitnik et al., Nuclear Instruments and Methods in Physics Research A 538 (2005) 431– 441.